Analytical representation of the fault slip velocity from spontaneous dynamic earthquake models

Andrea Bizzarri[1]

Received 14 December 2011; revised 11 May 2012; accepted 12 May 2012; published 20 June 2012.

[1] We have analyzed the most relevant features of three different analytical representations of the time evolution of the cosesimic slip velocity derived from theoretical basis; the so-called modified Yoffe function (MY), which pertains to a singular crack solution, the solution for a nonspontaneous crack obeying a position-weakening governing equation (PR) and the solution for a 1-D fault model subject to a linear slip-weakening friction law (B). By considering the same input parameters, we quantitatively compare these slip velocity functions (SVF) and we found that the time evolutions of the velocity and the correspondent slip predicted by the MY and B functions are very similar, while the PR predicts a very sharp peak. Correspondingly, the PR SVF is richer in high frequency and the fall off of its spectrum at high frequencies goes roughly as $\omega^{-1.5}$, while those of MY and B more closely follow ω^{-2}. Then we select two spontaneous, 3-D, dynamic, subshear models, representing a crack-like or a pulse-like rupture and we account for both homogeneous and heterogeneous configurations. We then compare the three SVF in order to see how they are able to reproduce the 3-D solutions; we also show how the input parameters of the SVF can be constrained from the results of the dynamic models. In the homogeneous cases our results indicate that the MY and the PR SVF reproduce adequately well the main features of a dynamic solution in the case of a crack-like rupture. The PR function overestimates v_{peak} and the MY SVF predicts a too rapid deceleration. In the case of a pulse-like rupture both the MY and the B SVF tend to underestimate v_{peak} , but all of them capture very well the final cumulated fault slip. Moreover, the B function fits better that the MY the overall behavior of the fault slip. The considered SVF are able to reproduce the spectral fall off of a 3-D solution at intermediate frequencies (for $\omega < 20$ Hz), the MY and the PR for a crack-like rupture and the MY and the B SVF for a pulse-like rupture. In particular, for $\omega < 10$ Hz the spectral content of the B function is practically indistinguishable from that of the spontaneous pulse-like solution. In the heterogeneous configurations the analytical functions cannot reproduce all the spectral details of the numerical solutions, but we see how it is possible to fit the overall behavior of a single pulse in fault the slip velocity time history. The thorough analysis performed in this work can contribute to the discussion about the debated choice of the source time function to be used in the kinematic models, which in turn is extremely important in the contest of hazard assessment and ground motions generation, although stress heterogeneities, geometrical irregularities, attenuation and free surface effects can definitively smear the details of the analytical functions.

Citation: Bizzarri, A. (2012), Analytical representation of the fault slip velocity from spontaneous dynamic earthquake models, *J. Geophys. Res.*, *117*, B06309, doi:10.1029/2011JB009097.

1. Introduction

[2] It is well known that spontaneous (i.e., without prior assigned rupture speeds), dynamic rupture problems for extended 3-D faults do not have closed-form analytical solutions, even in homogeneous conditions [*Bizzarri*, 2011b]. The only possible exception is represented by the 2-D, purely in-plane case [see *Kostrov*, 1974], even if a large number of integrals have to be solved numerically so that the advantage

[1]Istituto Nazionale di Geofisica e Vulcanologia, Sezione di Bologna, Bologna, Italy.

Corresponding author: A. Bizzarri, Istituto Nazionale di Geofisica e Vulcanologia, Sezione di Bologna, Via Donato Creti 12, I-40128 Bologna, Italy. (bizzarri@bo.ingv.it)

0148-0227/12/2011JB009097

Table 1. Synoptic Comparison of the Most Important Features of the Considered Slip Velocity Functions

Feature	Modified Yoffe (MY) Equation (1)	Palmer and Rice (PR) Equation (12)	Bizzarri (B) Equation (15)
Number of functions building the equation of the SVF	7	1	2
Class of continuity $\mathscr{C}^1$	yes	yes	yes
Number of free parameters	3	6	7
Free parameters	u_{tot}, t_R, t_S	v_S, v_P, G, $\Delta\tau_b$, v_r, E_G	v_S, G, m, k, v_0, $\Delta\tau_b$, E_G
Range of allowed rupture speeds	$0 \le v_r \le v_S$[a]	$0 \le v_r \le v_R$ in mode II $0 \le v_r \le v_S$ in mode III	$0 \le v_r \le v_S$[b]
Modeling of the short range slip healing	yes	no	yes
Explicit control of the slip duration, t_{pulse}	yes, equation (4): $t_R + 2\,t_S$	n/a	no; see equation (23)
Explicit control of the peak slip velocity, v_{peak}	yes, approximate estimate from equation (5): $0.9\frac{u_{tot}}{t_R^{0.47}\,t_S^{0.54}}$	yes, approximate estimate from equation (14): $1.52\frac{\Delta\tau_b}{G}\,\frac{v_r}{F(v_r)}$	no; see equation (24)
Explicit dependence on the properties of the medium surrounding the fault	no	yes	yes
Explicit dependence on the energetics of the system (breakdown stress drop / fracture energy density)	no	yes	yes

[a]The Yoffe function, modified as described in section 2, represents the solution for a mode III crack [see also *Nielsen and Madariaga*, 2003].
[b]The expression of c for the radiation damping term (see equation (16)) is formally appropriate for the mode III propagation.

of using an analytical approach partially vanishes. The dynamic modeling of earthquake ruptures thus relies on numerical models, which can also handle heterogeneous configurations and additional complications, expressed in terms of the fault geometry, the presence of multi-phase materials, the stress interaction phenomena, etc.

[3] On the other hand, the kinematic description of the earthquake processes needs the introduction of the so-called source time function, which is a proxy of the true slip velocity history arising from a dynamic (forward) model of the earthquakes. In the literature a large number of functions has been introduced; far of being exhaustive, we mention here the Dirac delta function, the box-car, the Gaussian, the Yoffe function, the Gabor signal, the Bouchon-ramp, the power laws [*Yoffe*, 1951; *Bouchon*, 1981; *Cotton and Campillo*, 1994; *Liu and Archuleta*, 2004]. Some of these functions are singular, others not ballistic, but nevertheless some of them have been widely used for their inherent simplicity and because their numerical implementation is straightforward, others for ad hoc choices to reproduce specific features of the rupture models and others for theoretical reasons [*Nakamura and Miyatake*, 2000; *Piatanesi et al.*, 2004]. Indeed, as pointed out in many papers [e.g., *Hisada*, 2000, 2001; *Guatteri et al.*, 2003; *Page et al.*, 2005], the arbitrary choice of the source time function has relevant effects in the resulting ground motions generation and therefore it plays a fundamental role in the contest of the strong motion prediction and hazard assessment.

[4] In this paper we consider three rather different, non-singular slip velocity functions (SVF henceforth) proposed in the literature, with the special aim to clarify whether they are able to reproduce the most important features of the time evolution of the fault slip velocity resulting from spontaneous, dynamic rupture models. All the considered functions are not arbitrary mathematical equations, but they have a strong theoretical basis; the first is a modification of the Yoffe function (proposed by *Tinti et al.* [2005]), originally expressing the solution for the Kostrov problem [*Kostrov*, 1964; *Nielsen and Madariaga*, 2003]. The second comes from the solution found by *Palmer and Rice* [1973] for a crack propagating with a fixed rupture speeds under the position-weakening friction law. The third function represents the solution for the 1-D dynamic problem for a fault governed the linear slip-weakening constitutive model. We will describe in detail these functions in sections 2 to 4; Table 1 compendiously summarizes the prominent features of these SVF.

[5] Then we quantitatively compare these SVF in section 5. The most ambitious goal of the paper (i.e., try to reproduce with these SVF a given fault slip velocity time history as resulting from a spontaneous spreading rupture over an extended fault) is pursued in sections 6, 7 and 8 where we consider two rather different behaviors, a crack-like rupture (section 6) and a pulse-like rupture (section 7). (For a formal definition of crack-like and pulse-like the reader can refer to section 2.2.4 of *Bizzarri* [2011b].) In section 8 we also consider a heterogeneous case, where the frictional properties are spatially variable. Finally, the last section of the paper summarizes the conclusions of the present study.

2. The Modified Yoffe Function

[6] Self-healing ruptures (characterized by a slip velocity time history having a compact support, i.e., vanishing after a time interval) were early investigated by *Yoffe* [1951], who found a steady state solution for a fixed width, propagating pulse in the mode I of rupture (i.e., for opening cracks). This solution, which has been further extended by *Broberg* [1978,

1999] and *Freund* [1979] to the mode II crack propagation, is singular at the crack tip, because it reads

$$v^{(\mathrm{Y})} = \frac{2}{\pi\, t_R}\mathrm{H}(t)\mathrm{H}(t_R - t)\,\sqrt{\frac{t_R - t}{t}}$$

where H(.) is the Heaviside function and t_R is the risetime (or slip duration) and t the time after the rupture onset. *Tinti et al.* [2005, equation (3)] propose a regularization of such a function by convolving it with a triangular function. The modified Yoffe (MY thereinafter) function is characterized by 3 parameters, the total (cumulative) slip developed at the target fault node (u_{tot}), t_R and the half-duration of the applied smoothing operator (t_S). (These quantities are indicated with symbols $D_{\max}$, τ_R and τ_S, respectively, in *Tinti et al.* [2005].)

[7] When $t_R > 2\ t_S$ the resulting slip velocity function is expressed as the combination of seven different functions:

$$v^{(\mathrm{MY})}(t) = K \begin{cases} 0 & ,t < 0 \\ C_1 + C_2 & ,0 \le t < t_S \\ C_1 - C_2 + C_3 & ,t_S \le t < 2t_S \\ C_1 + C_3 + C_4 & ,2t_S \le t < t_R \\ C_3 + C_4 + C_5 & ,t_R \le t < t_R + t_S \\ C_4 + C_6 & ,t_R + t_S \le t < t_R + 2t_S \\ 0 & ,t \ge t_R + 2t_S \end{cases}, \quad (1)$$

where

$$K \equiv \frac{2u_{tot}}{\pi t_R {t_S}^2}, \quad (2)$$

which corrects equation (A.7) of *Tinti et al.* [2005],

$$C_4 \equiv \left(\frac{t_R}{4} + \frac{t}{2} - t_S\right)\sqrt{(t - 2t_S)\,(t_R - t + 2t_S)} - t_R\,(t_R - t + 2t_S)\arcsin\left(\sqrt{\frac{t - 2t_S}{t_R}}\right) - \frac{3{t_R}^2}{4}\arctan\left(\sqrt{\frac{t_R - t + 2t_S}{t - 2t_S}}\right) \quad (3)$$

which corrects equation (A.18) of *Tinti et al.* [2005], and the remaining functions C_1, C_2, C_3, C_5 and C_6 are listed in equations (A.15), (A.16), (A.17), (A.19) and (A.20) of *Tinti et al.* [2005], respectively. In (1), (3) and in all the above mentioned equations t should be interpreted as the time elapsed after the onset of slip, not as the absolute time.

[8] From its definition it is apparent that the MY function is specifically appropriate to describe a slip pulse, because it explicitly predicts the healing of slip after the duration

$$t_{pulse}^{(\mathrm{MY})} = t_R + 2t_S. \quad (4)$$

We finally note that, in spite of the multiple functions which build equation (2), $v^{(\mathrm{MY})}$ it is of class $\mathscr{C}^1$ (i.e., it is a continuous function with continuous time derivative).

[9] The peak slip velocity (v_{peak}) is realized in the interval $t_S \le t \le 2\ t_S$, more precisely it is realized at $t \cong 1.3\ t_S$ [*Tinti et al.*, 2005, equation (6)]. At this time the value of $v^{(\mathrm{MY})}$ from equation (1) is modulated by the factor u_{tot}, but it still depends on both t_R and t_S. Numerically, it has been found that

$$v_{peak}^{(\mathrm{MY})} \cong 0.9\,\frac{u_{tot}}{{t_R}^{0.47}\,{t_S}^{0.54}}. \quad (5)$$

Approximating the exponents above with square roots, by combining equations (4) and (5) it is possible to obtain the value of t_R necessary reproduce a slip velocity pulse with given t_{pulse} and v_{peak}:

$$t_R^2 - t_{pulse}\,t_R + 2\left(\frac{0.9u_{tot}}{v_{peak}}\right)^2 = 0, \quad (6)$$

where the larger root is appropriate for the case of $v^{(\mathrm{MY})}$ written as in equation (1) and the lower root refers to the case when $t_R < 2\ t_S$, for which a different form of $v^{(\mathrm{MY})}$ holds [*Tinti et al.*, 2005]. (Once t_R has been estimated from equation (6) the value of t_S can be obtained from equation (4).)

3. Nonspontaneous Solution for the Position-Weakening Model

[10] By considering a nonspontaneous model (namely, a rupture developing on a planar surface with a prior-assigned and constant rupture speed v_r) where the fault friction linearly decreases with the increasing distance x from the nucleation point [see *Bizzarri* [2011b, equation (24)], *Palmer and Rice* [1973] found a solution for the displacement discontinuity across the interface (i.e., the fault slip u; their equation (46)). Expressing the fault slip velocity as $v = v_r\ \mathrm{d}u/\mathrm{d}x$ we obtain

$$v^{(\mathrm{PR})}(t) = \frac{9}{8}\,\frac{v_r\,\bar{u}}{R_0}\left(2\sqrt{\frac{v_r\,t}{R_0}} + \left(1 - \frac{v_r\,t}{R_0}\right)\ln\left|\frac{1 + \sqrt{\frac{v_r\,t}{R_0}}}{1 - \sqrt{\frac{v_r\,t}{R_0}}}\right|\right), \quad (7)$$

where $\bar{u}$ is a characteristic displacement (formally defined by *Palmer and Rice* [1973, equation (8)]) and R_0 is the characteristic distance of the position-weakening model (which is the counterpart of the characteristic slip d_0 in the linear slip-weakening friction law [see *Bizzarri*, 2011b, equation (25)]. The left hand side of equation (8) of *Palmer and Rice* [1973] expresses the so-called fracture energy density E_G [see *Bizzarri*, 2010b, equation (1)] so that we can write

$$\bar{u} = \frac{E_G}{\tau_u - \tau_f}, \quad (8)$$

where τ_u is the upper yield stress and τ_f is the residual level of friction after the stress release.

[11] On the other hand, the distance R_0 can be expressed as [see *Poliakov et al.*, 2002]

$$R_0 = \begin{cases} \frac{9\pi}{16}\,\frac{G}{1-\nu}\,\frac{\bar{u}}{\tau_u - \tau_f} = \frac{9\pi}{16}\,\frac{G}{1-\nu}\,\frac{E_G}{(\tau_u - \tau_f)^2} & \text{, for mode II} \\ \frac{9\pi}{16}\,G\,\frac{\bar{u}}{\tau_u - \tau_f} = \frac{9\pi}{16}\,G\,\frac{E_G}{(\tau_u - \tau_f)^2} & \text{, for mode III} \end{cases} \quad (9)$$

Table 2. Parameters Adopted in the Comparison Between the SVF Presented in Section 5

Parameter	Value
Medium and Discretization Parameters	
Rigidity, G	27 GPa
S wave velocity, v_S	3 km/s
P wave velocity, v_P	5.196 km/s
Time step, Δt	2.78×10^{-4} s
Breakdown stress drop, $\Delta\tau_b = \tau_u - \tau_f$	12 MPa
Fracture energy density, E_G	0.6 MJ/m^2
Mass per unit fault surface, m	1.11×10^6 kg/m^2 [a]
Stiffness, k	7 MPa/m[a]
Initial fault slip velocity, v_0	0.1 mm/s

[a]For the adopted values of m and k the resulting period of the analog freely slipping system, $T = 2\pi\sqrt{m/k}$, equals 2.5 s.

where the last equalities exploit equation (8). As observed by *Rice* [1980], in the case of a dynamic rupture the quasi-static estimate R_0 expressed in equation (9) is replaced by

$$R = R_0 F(v_r) = \frac{9\pi}{16}\ \frac{G\ E_G}{(\tau_u - \tau_f)^2}\ F(v_r), \tag{10}$$

where $F(v_r)$ is a function of the rupture speed which depends on the rupture modes [cf. *Bizzarri*, 2010b, equation (8)]:

$$F(v_r) = \begin{cases} (1-\nu)\dfrac{4\alpha_S\alpha_P - (1+\alpha_S^2)^2}{\alpha_S(1-\alpha_S^2)} & \text{, for mode II} \\ \alpha_S & \text{, for mode III} \end{cases} \tag{11}$$

being $\alpha_S \equiv \sqrt{1 - \frac{v_r^2}{v_S^2}}$ and $\alpha_P \equiv \sqrt{1 - \frac{v_r^2}{v_P^2}}$. We emphasize that equation (10) holds for both mode II and mode III. (The inverse of the two functions F in equation (11) have been sometime indicated with symbols f_{II} and f_{III}, respectively, in previous literature [e.g., *Poliakov et al.*, 2002]). Substituting R_0 with R, from equation (7) simple algebra gets

$$v^{(\mathrm{PR})}(t) = \frac{2}{\pi}\ \frac{\Delta\tau_b}{G}\ \frac{v_r}{F(v_r)}\left(2\sqrt{\frac{v_r\, t}{R}} + \left(1 - \frac{v_r\, t}{R}\right)\ln\left|\frac{1+\sqrt{\frac{v_r\, t}{R}}}{1-\sqrt{\frac{v_r\, t}{R}}}\right|\right), \tag{12}$$

where we have introduced the breakdown stress drop $\Delta\tau_b = \tau_u - \tau_f$ [*Bizzarri*, 2011b, equation (12)]. Incidentally, we recall here that $R^{(\mathrm{II}),(\mathrm{III})}$ is linked to the stress intensity factor $K^{(\mathrm{II}),(\mathrm{III})}$ as it follows [e.g., *Poliakov et al.*, 2002]:

$$R^{(\mathrm{II}),(\mathrm{III})} = \frac{9\pi}{32}\left(\frac{K^{(\mathrm{II}),(\mathrm{III})}}{\Delta\tau_b}\right)^2. \tag{13}$$

Due to the definition of F it emerges that the analytical solution (12) fully covers the admissible range of rupture speeds for the mode III (for which the limiting velocity is v_S), but it describes only the sub-Rayleigh range for the mode II of propagation (note that $F < 0$ for $v > v_R$, v_R being the Rayleigh velocity; in other words, it does not allow to consider the supershear rupture propagation). The behavior of the ratio $v_r/\mathrm{F}(v_r)$ for v_P and v_S as in Table 2 is reported in next Figure 2b.

[12] In the remained of this paper we will refer to equation (12) as the PR slip velocity function. As for equation (1), also in equation (12) t represents the time elapsed after the onset of slip.

[13] Due to the analytical formulation of (12) it is not possible to express $v_{peak}^{(\mathrm{PR})}$ in a closed-form equation; a numerical estimate can be written as

$$v_{peak}^{(\mathrm{PR})} \cong 1.52\,\frac{\Delta\tau_b}{G}\,\frac{v_r}{F(v_r)}. \tag{14}$$

[14] Notably, a similar relation has been inferred from laboratory experiments of mode II cracks developing at relatively low speeds on granite samples by *Ohnaka et al.* [1987] (see also further discussions in *Ohnaka and Yamashita* [1989, equation (47)] and in *Ohnaka and Shen* [1999, equation (26)]. On the other hand, in his numerical experiments *Bizzarri* [2012a] shows that the dependence of v_{peak} on v_r is more than linear; this has been shown also in the case of supershear events, for which the SVF considered in the present study do not apply.

[15] Finally, we remark that equation (12) is a good example which illustrates that the introduction of a constitutive model characterized by a scale length (in this case the position-weakening law with the characteristic distance R_0) removes the $1/\sqrt{t}$ singularity at the crack tip.

4. Analytical Solution for the Slip-Weakening Friction Law

[16] By considering a 1-D spring-slider analog fault system subject to the linear slip-weakening friction law *Bizzarri* [2012b] founds a closed-form, analytical solution of the equation of motion, which reads:

$$v^{(\mathrm{B})}(t) = \begin{cases} \dfrac{v_0}{2D_2}\left(-(c-D_2)\exp\left(-\dfrac{(c-D_2)\ t}{2m}\right) + (c+D_2)\exp\left(-\dfrac{(c+D_2)\ t}{2m}\right)\right) & , t \le t_f \\ \dfrac{\exp\left(-\dfrac{c\,\tilde{t}}{2m}\right)}{4k\,m^2\,\omega}\left[4k\,m^2\,\omega\,v_f\cos(\omega\,\tilde{t}) - \left(2c\,k\,m\,v_f + c^2\,D_1 + 4\,D_1\,m^2\,\omega^2\right)\sin(\omega\,\tilde{t})\right] & , t > t_f \end{cases} \tag{15}$$

in which

$$\begin{aligned} c &\equiv \frac{G}{2v_S} && , [c] = \frac{\text{Pa s}}{\text{m}} \\ D_1 &\equiv d_0\, k - \Delta\tau_b && , [D_1] = \text{Pa} \\ D_2 &\equiv \sqrt{\frac{c^2 d_0 - 4m\, D_1}{d_0}} && , [D_2] = \frac{\text{Pa s}}{\text{m}} \\ \tilde{t} &\equiv t - t_f && , [\,\tilde{t}\,] = \text{s} \\ \omega &\equiv \frac{\sqrt{4k\, m - c^2}}{2m} && , [\omega] = \text{Hz} \end{aligned} \tag{16}$$

and v_0 is the sliding velocity at $t = 0$ (assumed to be equal to the velocity of the loading point in the mass-block model), m is the mass-equivalent of the fault (per unit surface; $m = k(T/2\pi)^2$, being T the vibration period of the frictionless oscillator), k is the elastic constant of the spring (accounting for the elastic medium cut by the fault surface), and the constant c expresses the so-called radiation damping term, introduced to simulate the energy lost as propagating seismic waves. In equation (15), referred to as B slip velocity function in the reminder of the paper, t_f is the time when the developed fault slip u first reaches the characteristic slip-weakening distance d_0 and v_f is the slip rate at this instant (v_f corresponds to the quantity v_0 in *Bizzarri and Cocco* [2003; see also their Figure 2a].

[17] As discussed in *Bizzarri* [2012b], the following conditions have to be met in order to have a real-valued function (i.e., an admissible solution) and an unstable behavior:

$$\begin{cases} D_1 < 0 \\ \omega \in \mathbb{R}_0^+ \end{cases} \Leftrightarrow \begin{cases} d_0 k - \Delta\tau_b < 0 \\ 4km - c^2 > 0 \end{cases}, \tag{17}$$

which can be rewritten in the compact form

$$\frac{c^2}{4\,m} < k < \frac{\Delta\tau_b}{d_0}, \tag{18}$$

which, for assigned $\Delta\tau_b$ and d_0, gives the maximum admissible value of k. (Incidentally we note that the first condition in (17) ensures that the constant D_2 in (16) is a real number.)

[18] There are some attempts to relate the stiffness of the spring-slider analog model to the "stiffness" of a seismogenic extended fault. *Walsh* [1971] proposed the following approximation

$$k \cong \frac{G}{W^f}, \tag{19}$$

where W^f is the fault width. Another possible estimation can be written as $k = 1/C$, where C is the local compliance [*Bizzarri et al.*, 2001] which represents the proportionality constant existing between the instantaneous traction and the fault slip. We can write [*Bizzarri and Cocco*, 2005]:

$$k = \frac{G}{4\omega_{CFL}{}^2\, \Delta x} \tag{20}$$

being ω_{FLC} the Courant-Friedrichs-Levy (CFL) ratio, $\omega_{FLC} = v_S\, \Delta t/\Delta x$ (where Δt and Δx are the spatial and temporal sampling, respectively). In the present paper we use the following relation [*Cao and Aki*, 1986], which directly relate the stiffness to two dynamic observables:

$$k = \frac{\Delta\tau_b}{u_{tot}}. \tag{21}$$

On the other hand, the quantity m can be approximated as

$$m = \rho\ l, \tag{22}$$

where ρ is the cubic mass density of the medium surrounding the fault and l is the effective fault thickness (in the direction perpendicular to the fault), approximated as $l \cong v_S\, t_{pulse}$ [*Yamashita*, 1976; *Cao and Aki*, 1986], where, as in equation (4), t_{pulse} expresses the risetime (or the slip duration). Note that l does not represent the half-thickness of the slipping zone characterizing the seismogenic fault zone (see section 2 in *Bizzarri* [2009b] and references cited therein).

[19] In equation (15) t is the time elapsed since $t_{first} = \tau_u/(k\ v_0)$, which formally defines the time when the frictional resistance of the fault, loaded by a constant loading rate $\dot{\tau}_{load} = kv_0$, first reaches the upper yield τ_u. Within the framework of the linear slip-weakening constitutive model this condition formally defines the onset of slip. Therefore the meaning of t for all the considered slip velocity functions (the MY of equation (1), PR of equation (12) and B of equation (15)) is exactly the same.

[20] Simple algebra shows that it is possible to obtain a closed-form expression for the slip duration

$$t_{pulse}^{(\mathrm{B})} = t_f + \frac{1}{\omega} \cdot \arccos\left(\frac{c^2\, D_1 + 2c\, k\, m\, v_f + 4D_1\, m^2\, \omega^2}{(c^2 + 4m^2\, \omega^2)\left(\left(c\, D_1 + 2k\, m\, v_f\right)^2 + 4D_1{}^2\, m^2\, \omega^2 \right)} \right), \tag{23}$$

but it is useless for practical purposes, in that t_f and v_f are a priori unknown. At the same time, also the peak slip velocity can be expressed in a closed-form:

$$\begin{aligned} v_{peak}^{(\mathrm{B})} &= v^{(\mathrm{B})}\left(\tilde{t} = \tilde{t}_{peak}\right) \\ \tilde{t}_{peak} &= \frac{1}{\omega} \cdot \arccos\left(s\, \frac{c^2\, \left(c\, D_1 + 2k\, m\, v_f\right) + 4m^2\, \omega^2\, \left(c\, D_1 - 2k\, m\, v_f\right)}{(c^2 + 4m^2\, \omega^2)\, \sqrt{\left(c\, D_1 + 2k\, m\, v_f\right)^2 + 4D_1{}^2\, m^2\, \omega^2}} \right) \\ s &\equiv \text{sign}\left(c^2\, D_1 + 4c\, k\, m\, v_f + 4D_1\, m^2\, \omega^2\right), \end{aligned} \tag{24}$$

but again it is useless because v_f is a priori unknown.

5. Numerical Results

[21] In this section we compare the different SVF described in sections 2 to 4, namely the MY (equation (1), the PR (equation (12)) and the B function (equation (15)). The most important features of these three SVF are presented in the synopsis of Table 1.

[22] To perform a quantitative comparison we adopt the parameters tabulated in Table 2. For the given value of E_G and $\Delta\tau_b$ we can also have the value of the characteristic slip-

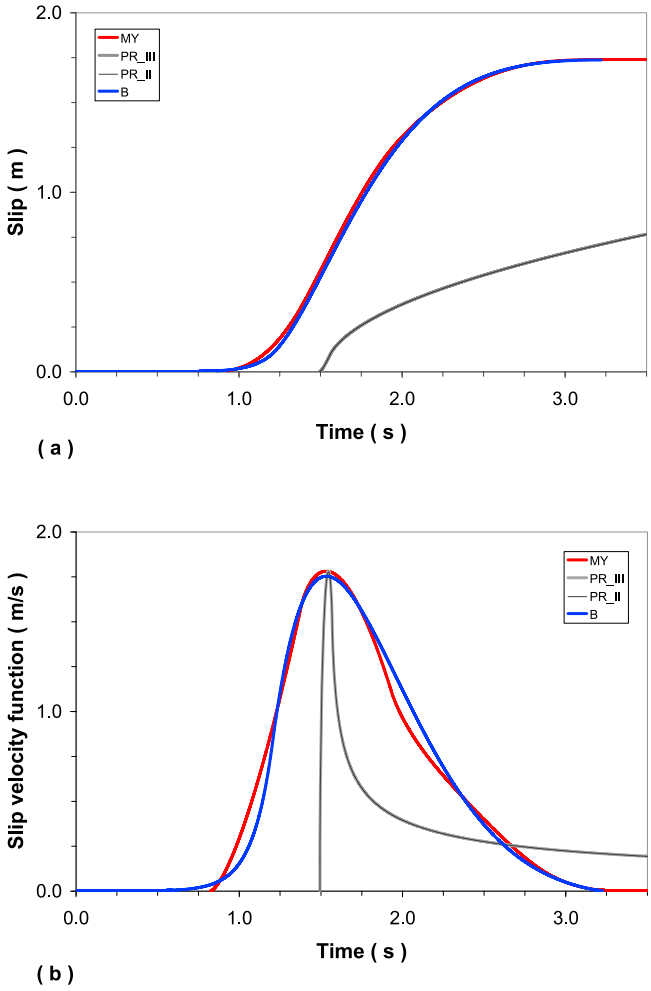

Figure 1. Comparison of the three different SVF considered in the present study, the MY (equation (1), the PR (equation (12)) and the B function (equation (15)). (a) Resulting cumulative fault slip. (b) Time evolution of the slip velocity. The adopted parameters are listed in Table 2. The remainder free parameters are: u_{tot} = 1.74 m, t_R = 1.436 s and t_S = 0.557 s for the MY and v_r = 2.247 km/s or 1.976 km/s, for the mode II or III, respectively, for the PR function. See section 5 for the details about this choice.

weakening distance d_0 appearing in equation (15); from *Bizzarri* [2010b, equation (2)] we have: d_0 = 0.1 m. First of all we compute the B function; it exhibits a total slip of 1.74 m and a peak of slip velocity of 1.75 m/s. We can also estimate the pulse duration as 2.55 s. To compute the MY we need to assign u_{tot} (which is 1.74 m) and the two free parameters t_R and t_S. They can be easily estimated through equations (4) and (6), from which we obtain t_R = 1.436 s, t_S = 0.557 s. Finally, to compute the PR we need to assign the rupture velocity v_r. From equation (14) we can found the value of the ratio $v_r/F(v_r)$ which makes $v_{peak}^{(PR)}$ equal to 1.75 m/s. Moreover, due to the definition of the function F (see equation (11)), we found numerically v_r = 2.247 km/s for the mode II and v_r = 1.976 km/s for the mode III. Finally we apply a time shift of 0.82 s and 1.5 s for the MY and the PR functions, respectively, in order to have the peak slip velocities coincident in all the cases.

[23] We emphasize that this is one possible method to associate the parameters of the different SVF, but it has not been chosen arbitrarily. Indeed, we note that it is not feasible to start the comparison from the PR function, because, by definition, it cannot give the total slip, which characterize the other two SFV. On the other hand, we cannot control a priori the value of the total developed slip predicted by the B function, so that it cannot be feasible to start the comparison from the MY SVF; we would have to search for the optimal parameters of the B function which produce the value of u_{tot} given by the MY. In conclusion, the proposed method is the most computationally convenient and it has precise motivations. Finally, we also recall here that one of the main purposes of the present study is to see whether it is possible to reproduce the time evolution of the fault slip velocity predicted by a dynamic rupture model with an analytical, theoretically-based SVF. For this reason we first assign the fracture energy density and the breakdown stress drop.

[24] The results are reported in Figure 1. We can clearly see that the peaks are practically identical, as expected from the choice of the parameters described above. Remarkably, we note a very good agreement between MY and B, not only concerning the pulse duration and the peak slip rate (which are imposed to be equal), but also concerning the shape of the functions (Figure 1b). The resulting fault slip (obtained by numerical integration of the SVF) are indistinguishable (see Figure 1a). The only difference is near the rupture onset; while the B function predicts a smooth increase of v, the MY predicts a more abrupt increase. After the peak, both these two SVF (MY and B) exhibit a very similar behavior; both of them has a flex at t = 1.72 s and both prescribe a very similar deceleration phase and the final healing of slip. On the other hand, we can clearly observe that the PR is definitively different; in spite of the identical peak in v, the resulting slip is quite different with respect the other two SVF (Figure 1a). This is not surprising, in that the PR function is penny shaped, it has a very abrupt increasing rate (i.e., it predicts a very high acceleration near the rupture onset). This also is not surprising, because the PR function refers to a model where the position-weakening constitutive law is known to produce a very fast acceleration stage once a fault node fails, as the slip-weakening law [e.g., *Bizzarri and Cocco*, 2003]. As it is well known, the most remarkable difference is that the PR SVF does not predict the healing of slip, but if describes a crack-like rupture (see section 2.2.4 in *Bizzarri* [2011b] for a discussion).

[25] From the comparison between the PR and the other two SVF it emerges that the time interval between the onset of the rupture ant the peak in slip velocity is very small (5.24×10^{-2} s). Basing on the method proposed by *Fukuyama et al.* [2003], *Mikumo et al.* [2003] propose to estimate the value of the characteristic distance over which the traction degrades as the time integral of the fault slip velocity for the onset of the rupture up to its peak, because they assume that at that instant the traction is completely release and the final, kinetic level is reached. By computing this integral for the case of the PR function we obtain the value of 0.073 m, which is slightly smaller than the value of d_0 = 0.1 m resulting from the prescribed value of E_G and $\Delta\tau_b$. However, we emphasize two things. First, the curve reported in Figure 1 is what it results from the assumption of the two input parameters E_G and $\Delta\tau_b$, which enter directly in

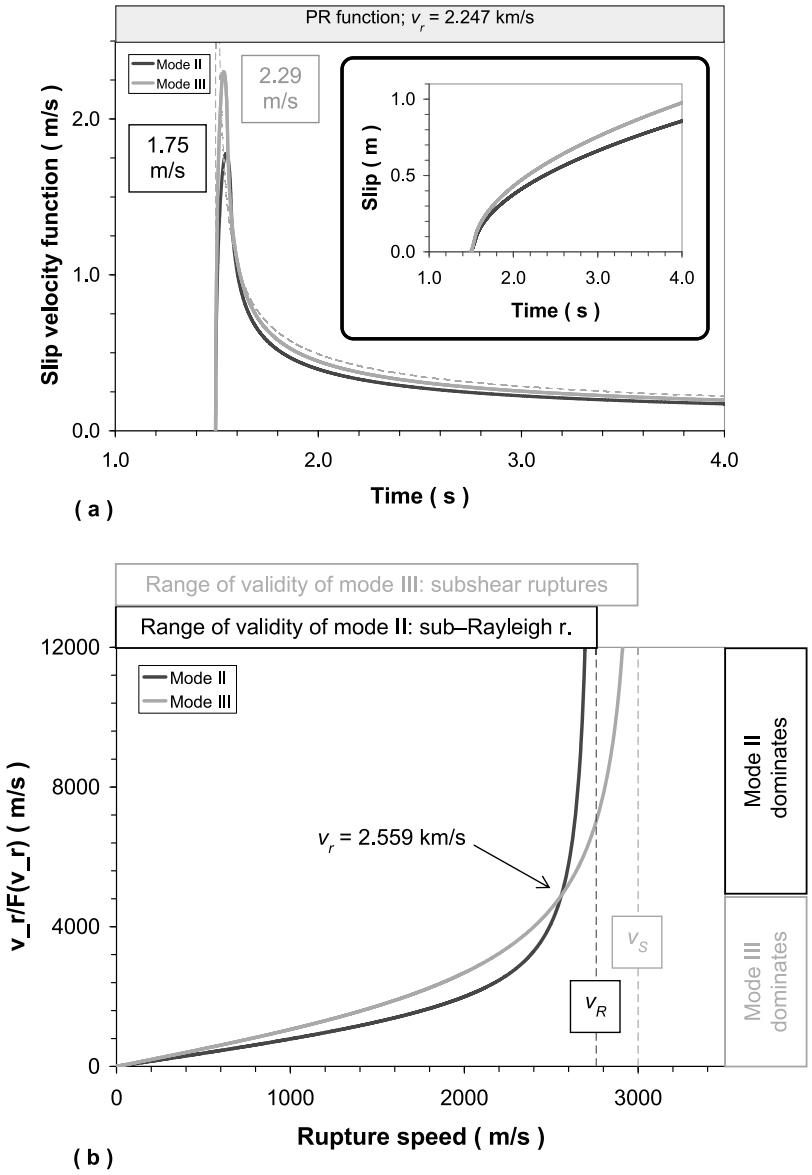

Figure 2. (a) Comparison between the mode II and the mode III versions of the PR function. The parameters are the same as for Figure 1, but now v_r = 2.247 km/s in both the cases. Dashed gray line represents the singular solution for the mode III case [see *Andrews*, 1976]. (b) Behavior of the ratio $v_r/F(v_r)$ for v_P and v_S as in Table 2. The vertical dashed lines represent the limiting rupture speeds where the function F diverges (see equation (11)).

the analytical expression of the PR SFV (recall equation (10)). Second, and more importantly, we emphasize that the method of *Mikumo et al.* [2003] has been proven to be adequate in the case of supershear ruptures, but it gives an underestimate of d_0 in the case of subshear events [*Tinti et al.*, 2004; *Bizzarri*, 2010a, 2012c].

[26] An interesting result is that the condition to have a given peak of v causes the mode II and mode III versions of the PR function to be identical. Indeed, from equation (14) we have selected the same value of the ratio $v_r/F(v_r)$; this is realized for two different values of v_r (depending on the rupture mode), but it gives exactly the same behavior of the PR function in the two modes (recall its definition in equation (12); the constant $v_r/F(v_r)$ appears as a multiplier factor and the quantity $v_r\ t/R$ is proportional to $v_r/F(v_r)$; see equation (10)). On the other hand, we emphasize that for the same value of the rupture speed the PR function predicts that the peak of v in mode III is greater than that in mode II (see Figure 2a). This theoretical result has been also obtained numerically in 3-D for many governing equations [see *Bizzarri*, 2011a, Figures 3c and 3d; *Bizzarri*, 2012a, Figures A1 and A2], confirming early results for a 2-D mixed-mode rupture obeying the linear slip-weakening friction law [*Andrews*, 1994]. We also emphasize that the predominance of the mode III with respect to the mode II is not true in general; from Figure 2b we can clearly see that in the range of admissible rupture speeds, the mode III dominates up to a critical velocity (for the Poissonian medium

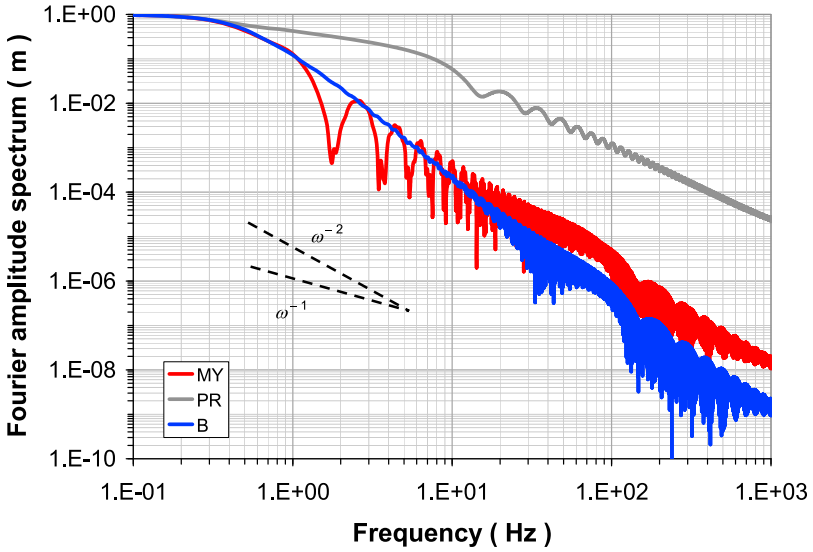

Figure 3. Fourier amplitude spectra (FAS) of the three SVF plotted in Figure 1. All the time histories have been normalized to unit fault slip and therefore in the zero frequency limit all the FAS converge to the same value.

considered here, this critical value is 2.559 km/s), and then the mode II dominates up to the limiting speed of v_R.

[27] Moreover, from Figure 2 it emerges that the decreasing part of v described by the PR SVF closely resembles the well-known singular solution. Indeed, the dashed gray line in Figure 3 represents the function $v = C(t - t_r)^a$, where C is a constant, t_r is the rupture time and a equals to 1/2 in the sub-Rayleigh case [*Andrews*, 1976; see also *Burridge*, 1973].

[28] In Figure 3 we report the Fourier amplitude spectrum (FAS) of the different time histories of v reported in Figure 1. We normalize to unit slip all the three time series; in the case of the crack-like function (i.e., PR) we sinus-taper it, following the same strategy of *Bizzarri and Spudich* [2008], in order to obtain a null value of the velocity after 2.55 s. The similarity of MY and B discussed above reflects in very similar spectra; the high frequency content is nearly the same for both the MY and the B SVF for frequency up to roughly 5 Hz, and for greater frequencies the MY function is richer in high frequency content. On the other hand, the PR SVF has a higher FAS; this is justified by considering that it is penny shaped, as observed above (Figure 1b). The spectra of MY and B functions have a comparable fall off at high frequency; we can estimate a behavior of $\omega^{-\alpha}$ with α slightly greater than 2 for the MY and roughly equal to 2.2 for the B SVF. On the contrary, the PR function exhibits a fall off proportional to $\omega^{-1.5}$.

[29] In full of generality we can chose parameters which guarantee that the PR SVF resembles more closely the MY and the B functions. Just for an example, in Figure 4a we report the time evolution of the PR function where we have changed both the fracture energy density and the breakdown stress drop (now we have: $E_G = 1$ MJ/m^2 and $\Delta\tau_b = 3$ MPa). As a consequence also d_0 is changed with respect to the value adopted in Figure 1; now we have: $d_0 = 0.67$ m. Again, the value of v_r has been chosen in order to obtain the same peak slip rate predicted by the other two SVF (in this case we obtain $v_r = 2.882$ km/s for mode III). Finally we apply the time shift of 1.17 s to have the coincidence of the peaks. In this case the PR function is not so picked as in the previous case; correspondingly the FAS (see Figure 4b) has a reduced high frequency content compared to the previous case of Figure 3. Also the fall off at high frequencies is now closer to the ω^{-2}, which roughly describes the behavior of the MY and B SVF. We can also note from the inset in Figure 4a that the slip predicted by the PR function is now very similar to the other two. However, it is important to remark here that to obtain this better comparison with the other two SVF we have chosen a different parameter setting, in that both E_G and $\Delta\tau_b$ have to be changed ad hoc.

6. Representation of Solutions From Spontaneous 3-D Ruptures: A Crack-Like Solution

6.1. Spontaneous Modeling

[30] Once the prominent features of the three considered SVF has been explored (see section 5) the following intriguing question naturally emerges: is it possible to fit a solution from a spontaneous dynamic earthquake model with the SVF presented above? In general, we can anticipate that the agreement could not be in principle fully satisfactory, in that all the three SVF do not include the whole physics of the cosesimic process. This will be true especially in the case of heterogeneous configurations (which will be considered in section 8), in that the SVF come from idealized, homogeneous models. As we will see, for these heterogeneous models we expect to have a mismatch in the frequency domain between the analytical SVF and the numerical solutions. Basically, the MY refers to a mode III pulse-like solution, the PR to a crack obeying to position-weakening friction and the B function pertains to a 1-D rupture governed by slip-weakening constitutive law. On the other hand, it must be recalled that if ruptures are energetically comparable, it would be very difficult to distinguish among two different governing models, also considering the frequency content of the solutions [*Bizzarri*, 2011b].

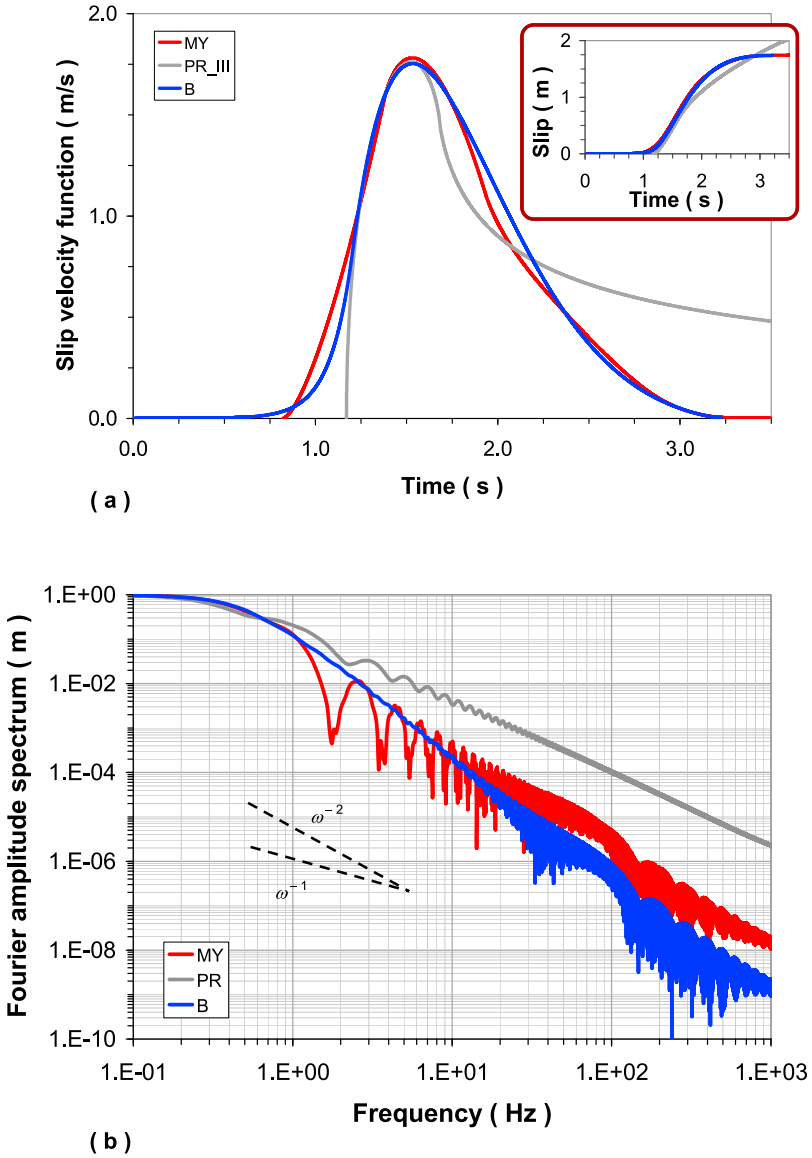

Figure 4. (a) The same as Figure 1, but now in the case of PR SVF we adopt $E_G = 1$ MJ/m^2, $\Delta\tau_b = 3$ MPa and $v_r = 2.882$ km/s. The inset reports the time evolution of the slip. (b) FAS of the time series of Figure 4a. Red and blue curves are exactly those of Figures 1 and 3.

[31] In order to answer to the previous question we consider first (present section and section 7) the fault slip velocity time histories resulting from 3-D spontaneous model of earthquake ruptures, spontaneously developing on vertical planar faults, with homogeneous properties. (As already mentioned, we will consider an example of heterogeneous rupture in section 8.) In Table 3 is summarized the logical scheme used to constrain the free parameters of each single SVF from the results pertaining to a dynamic rupture model.

[32] Here we consider the solution reported in Figure 5, which is obtained by assuming the Ruina-Dieterich governing model [*Bizzarri*, 2011b, equation (35)] with the parameters listed in *Bizzarri* [2009a, Table 1]. The rupture behaves as a sub-Rayleigh one, as we can see from the distribution of the rupture speeds (see Figure 5a). We select a fault node located in the anti-plane direction (the point R in Figure 5a), at a distance of 3 km from the hypocenter; in this point the rupture is fully developed and there is no influence of the nucleation procedure (which is described in *Bizzarri* [2009a]). We will discuss how the results can be affected by the choice of a different fault receiver in Appendix A.

[33] The rupture exhibits a crack-like behavior, in that the slip velocity does not fail to zero, but it remains at a value of v_2 (see Figure 5b). We will explore in section 7 the case of a pulse-like rupture. The present model represents an earthquake having a seismic moment $M_0 = 9.4 \times 10^{17}$ Nm, which corresponds to a magnitude $M_w = 5.9$, as the earthquake which strokes the Emilia region, northern Italy, May 20, 2012.

[34] In Figure 5c we report the behavior of the traction as a function of the cumulated fault slip (i.e., the slip-weakening curve); from this plot we can estimate the equivalent upper yield stress (τ_u^{eq}) and the equivalent residual level (τ_f^{eq}),

Table 3. Schematic Summary of the Logical Scheme Used to Compare the Various SVF With a Numerical Solution[a]

SVF	Crack-Like Rupture	Pulse-Like Rupture
Modified Yoffe (MY) equation (1)	t_{peak} v_{peak} u_{tot} : u at t when $v = v_2$ (asymptotic value) $t_S = \frac{t_{peak} - t_r}{1.3}$ $t_R = \frac{1}{t_S}\left(\frac{0.9 u_{tot}}{v_{peak}}\right)^2$ check if $t_R > 2\ t_S$	t_{peak} t_{pulse} u_{tot} $t_S = \frac{t_{peak} - t_r}{1.3}$ $t_R = t_{pulse} - 2\ t_S$
Palmer and Rice (PR) equation (12)	v_r $\Delta\tau_b$ $E_G = \int_0^d (\tau - \tau_{res})\mathrm{d}u$ where: $\tau_{res} = \tau_f$ or $\tau_u^{eq} - 0.95\ \Delta\tau_b$; d: u when $\tau = \tau_{res}$	n/a
Bizzarri (B) equation (15)	n/a	t_{pulse} u_{tot} $v_0 \equiv v(t = t_r)$ $\Delta\tau_b$ $k = \frac{\Delta\tau_b}{u_{tot}}$ $m = \rho\ v_S\ t_{pulse}$

[a]For each SVF some quantities have to be retrieved from the numerical solution and used to compute its free parameters. The rupture time t_r has to be always derived from the dynamic model. This procedure has been applied in sections 6 to 8. Readers can refer to Figures 5b, 5c, 7b and 7c for the interpretation of the various quantities mentioned.

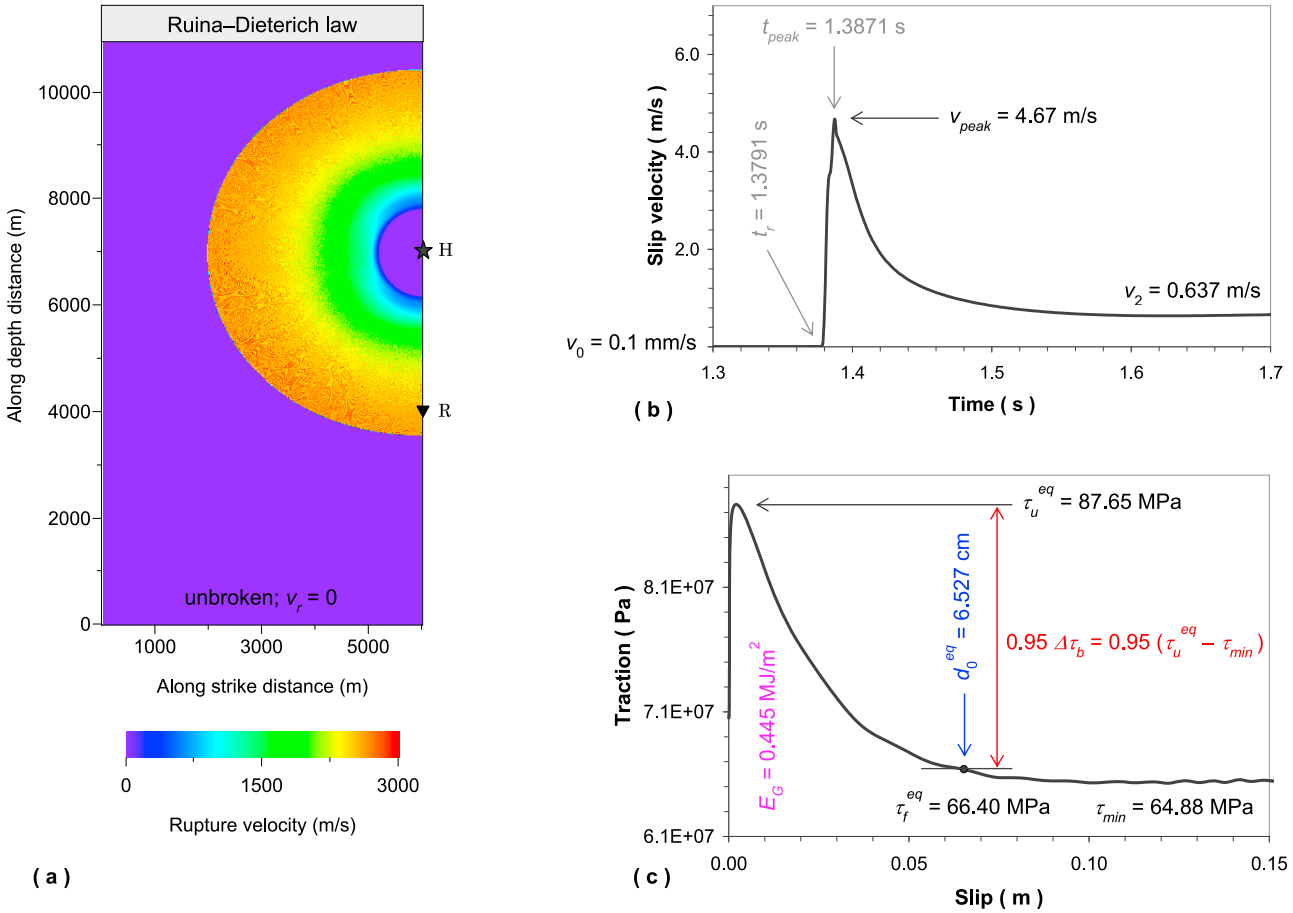

Figure 5. Solution for a spontaneous rupture obeying the Ruina-Dieterich governing model [see *Bizzarri*, 2011b, equation (35)]. (a) Distribution of the rupture speed (v_r) on the fault plane (note that, due to symmetry conditions of the bilaterally expanding rupture only one half of the fault surface is reported). We compute v_r as in *Bizzarri* [2011b, equation (16)], H denotes the hypocenter, and R the fault node where the solution of Figures 5b and 5c are plotted; R is located in the anti-plane direction at a distance of 3 km from H. The purples region behind H indicates the nucleation region (see *Bizzarri* [2009a] for numerical details). (b) Time history of the fault slip velocity. (c) Resulting slip-weakening curve. In Figures 5b and 5c the relevant values of the dynamic model are also given (see section 6.1 for details).

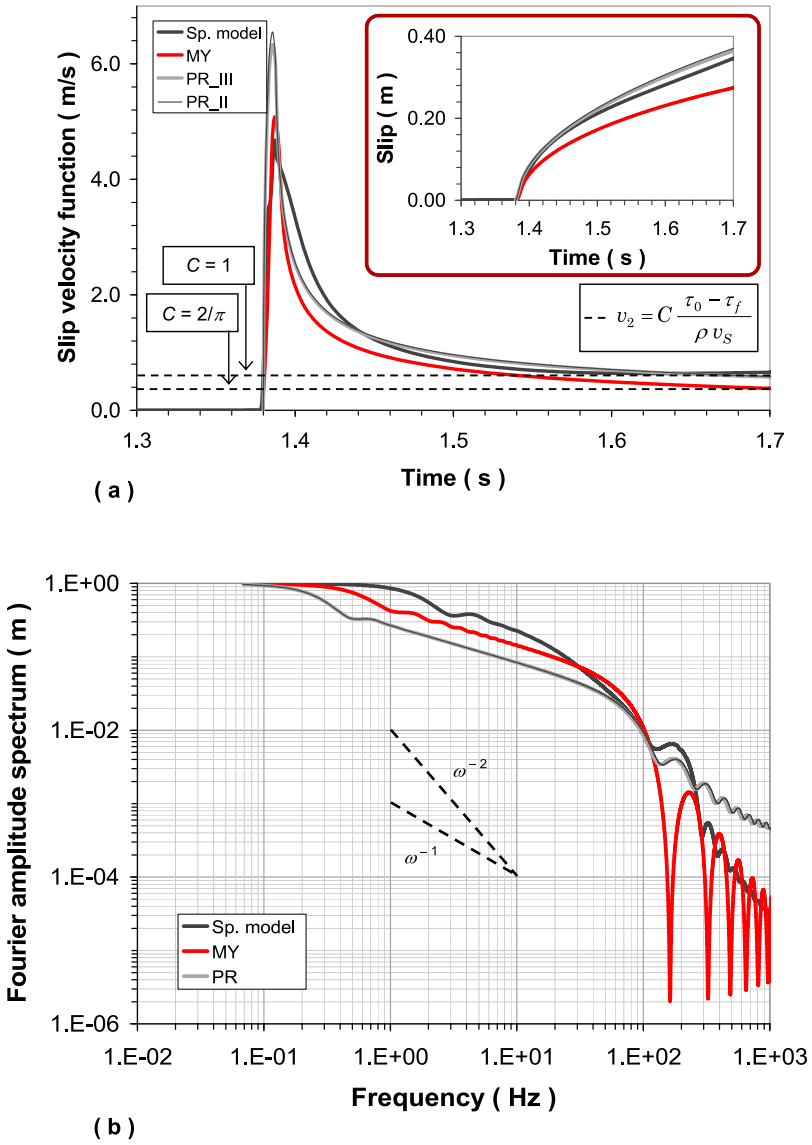

Figure 6. (a) Comparison between the fault slip velocity in the receiver R for the spontaneous crack-like model of Figure 5 against the MY and the PR SVF. We report as dashed lines the asymptotic values of final velocity v_2 are predicted by the shear impedance relation (equation (25)). (b) Comparison between the resulting Fourier amplitude spectra.

which are the counterparts of τ_u and τ_f, respectively, in the framework of the position- and slip-weakening constitutive models [*Bizzarri and Cocco*, 2003]. The fault weakening is not linear, but more closely resembles an exponential decrease as the fault slip increases. We therefore estimate the equivalent slip-weakening distance (d_0^{eq}) as the slip cumulated up the time when the traction drop equals the 95% of the breakdown stress drop ($\Delta\tau_b = \tau_u^{eq} - \tau_{\min}$; see Figure 5c). Correspondently, we compute the E_G from *Bizzarri* [2010b, equation (1)], with $d = d_0^{eq}$ and $\tau_{res} = \tau_f^{eq} = \tau_u^{eq} - 0.95\ \Delta\tau_b$.

6.2. Representation Through the MY Function

[35] From the difference between the time when the fault slip velocity peak is attained and the rupture time (t_{peak} and t_r, respectively, in Figure 5b) we have the measure of the duration of the acceleration phase of the rupture. As previously discussed this gives us the possibility to estimate the parameter t_S of the MY: $t_S = (t_{peak} - t_r)/1.3 = 6.15 \times 10^{-3}$ s, which roughly corresponds to 14 time levels (owing to the good spatio-temporal resolution of the dynamic model). As mentioned above, the spontaneous model does not exhibit a saturation slip, but a possible choice for the parameter u_{tot} of the MY function is the slip at $t = 1.8$ s, where the slip velocity has reached its asymptotic value v_2 (see Figure 5b); we have $u_{tot} = 0.4$ m. Then we can estimate the remaining parameter, t_R by solving equation (6), in which we recall that $t_{pulse} = t_R + 2\ t_S$ (equation (4)) and where u_{tot} and v_{peak} are known quantities. We therefore obtain: $t_R = \frac{1}{t_S}\left(\frac{0.9u_{tot}}{v_{peak}}\right)^2 = 0.977$ s, which is greater than $2\ t_S$, so that the formulation of equation (1) is correct. The resulting t_{pulse} is then 0.989 s and the result is reported in red in Figure 6.

6.3. Representation Through the PR Function

[36] The choice of the values of the parameters of the PR function (equation (12)) is straightforward, in that all the quantities are known. Indeed, from the spontaneous simulation we know that the rupture speed in R is $v_r = 2.573$ km/s. Interestingly, this value slightly exceeds the critical threshold of 2.559 km/s over which the mode III is no longer paramount with respect to the mode II in the framework of the PR representation of the rupture (see Figure 2b).

[37] The result pertaining to the PR function is reported in gray in Figure 6. Even if the motion in R is basically anti-plane, just for completeness we have also considered the mode II version of the PR function, which is reported as thin gray curve in Figure 6.

6.4. Discussion

[38] From the comparison of the curves in Figure 6a it clearly emerges that the peaks of the slip rate are attained at the same instant; this is prescribed in the case of the MY function (red curve), but not in the case of the PR function (gray and thin black curves).

[39] Remarkably, the final values of velocity are comparable in all cases; in Figure 6 we also superimpose the final velocity as predicted by the shear impedance relation [*Scholz*, 1990; *Bizzarri and Cocco*, 2003], which reads:

$$v_2 = C\,\frac{\tau_0 - \tau_f}{\rho\, v_S} \tag{25}$$

C being a dimensionless constant ranging from 1 to $2/\pi$ as v_r increases from 0 to v_S. The two extreme values of this estimate are, considering that in the spontaneous model $\tau_0 = 70.52$ MPa and putting $\tau_f = \tau_f^{eq}$ in (25), $v_2 = 0.582$ m/s and $v_2 = 0.371$ m/s. These values are reported as dashed lines in Figure 6a. The spontaneous model agrees very well with the case of $C = 1$, which is also the asymptotic value in the case of the PR SVF.

[40] As discussed above (see section 6.3), for the rupture speed in the target fault receiver the time evolutions of the two versions of the PR function (in-plane and anti-plane) are quite similar. Both of them overestimate v_{peak} predicted by the spontaneous model. On the contrary, the MY function (red curve) fits reasonably well the peak slip velocity.

[41] We also emphasize that the agreement between the crack-like spontaneous rupture (black line in Figure 6a) and the MY function is not obvious; indeed, the MY is specifically designed to represent pulse-like ruptures. This example clearly shows that, once v_{peak} and its time occurrence are constrained, the resulting parameters of the MY SVF make it possible to reproduce a crack-like rupture. Of course, this agreement is limited to a specific time window; while the spontaneous model and the PR function predict a similar, nonzero asymptotic value of v, the MY predicts the healing of slip (for the adopted parameters this occurs at $t = t_r + t_{pulse} = 2.3681$ s).

[42] Concerning the evolution of the slip we can conclude that the PR functions are able to reproduce very well the spontaneous model (see the inset in Figure 6a). On the contrary, the MY predicts a lower slip; this can be imputed to the choice of the parameter u_{tot}, which in the case of a crack-like rupture is somehow arbitrary, contrarily to the case of a pulse-like rupture, were this is a well-defined and measurable quantity.

[43] In Figure 6b we report the FAS of the four time series of Figure 6a. It emerges that below 30 Hz the PR function is poorer in high frequency compared to the spontaneous model and that the MY function is in the middle of the two. In this frequency range the overall behavior is $\sim\omega^{-1}$, in agreement with the findings of *Bizzarri and Spudich* [2008]. Moreover, at high frequencies we can see that the FAS of the PR function is paramount with respect to that of the MY SVF, as also observed in Figures 3 and 4b. Moreover, we have that at very high frequencies the fall off of the spectra roughly is ω^{-2} for the MY and $\omega^{-1.5}$ for the PR function (as in Figure 3). The fall off of the spontaneous solution is somehow in between these two fall offs, more close to that of the MY function.

7. Another Example: A Pulse-Like Rupture

7.1. Spontaneous Modeling

[44] In this section we consider an earthquake model in which the slip heals, leading to vanishing final fault slip velocity. In this case the fault obeys a rate-, state- and temperature-dependent friction law [*Bizzarri*, 2011b, equation (48)], which is known to represent a suitable mechanism to simulate the pulse-like propagation. Also this synthetic earthquake is a subshear event (see Figure 7a). The adopted parameters are the same as in *Bizzarri* [2010a], which in turn correspond to those used to generate the crack-like rupture described in section 6.1. As thoroughly discussed in *Bizzarri* [2010a], the explicit dependence on the temperature developed by frictional heat, provided that the deformation is concentrated in a sufficiently thin slipping zone, causes the fault to experience a fast restrengthening after the dynamic stress drop (see Figure 7c). In turn, this causes the slip to heal; this occurs at time $t_h = 1.33$ s (Figure 7b), which leads to a pulse duration $t_{pulse} = 0.4271$ s. The peak slip velocity is comparable with the previous model (compare Figures 5b and 7b), and does not assume the large values typically realized in other pulse-like rupture (see for instance the flash-heating mechanism, which is known to predict $v_{peak} \sim 10$ s of m/s [*Bizzarri*, 2009a]). The total cumulative slip in R is: $u_{tot} = 0.111$ m. This value is small, compared to supershear, crack-like earthquakes developing on long faults, for which we can expect values of slip of some meters. The event considered here is of moderate size; its seismic moment is $M_0 = 1.5 \times 10^{17}$ Nm, which corresponds to a magnitude $M_w = 5.4$.

7.2. Representation Through the MY Function

[45] Due to the pulse-like nature of the rupture, in this case the choice of the parameter u_{tot} is well constrained. Moreover, from Figure 7b we can estimate, in the same manner as in section 6.2, $t_S = (t_{peak} - t_r)/1.3 = 1.28 \times 10^{-2}$ s. Finally, from equation (4), by using the pulse duration mentioned above (section 7.1) and the value of t_S just computed we obtain the value of the third parameter of the MY function: $t_R = 0.4018$ s. The resulting curve is reported in red in Figure 8a.

[46] A second choice we made to fit the spontaneous solution of our 3-D fault model with the MY SVF consists in prescribing u_{tot} and t_S exactly as described above, but constraining v_{peak} instead of the effective pulse duration. This is

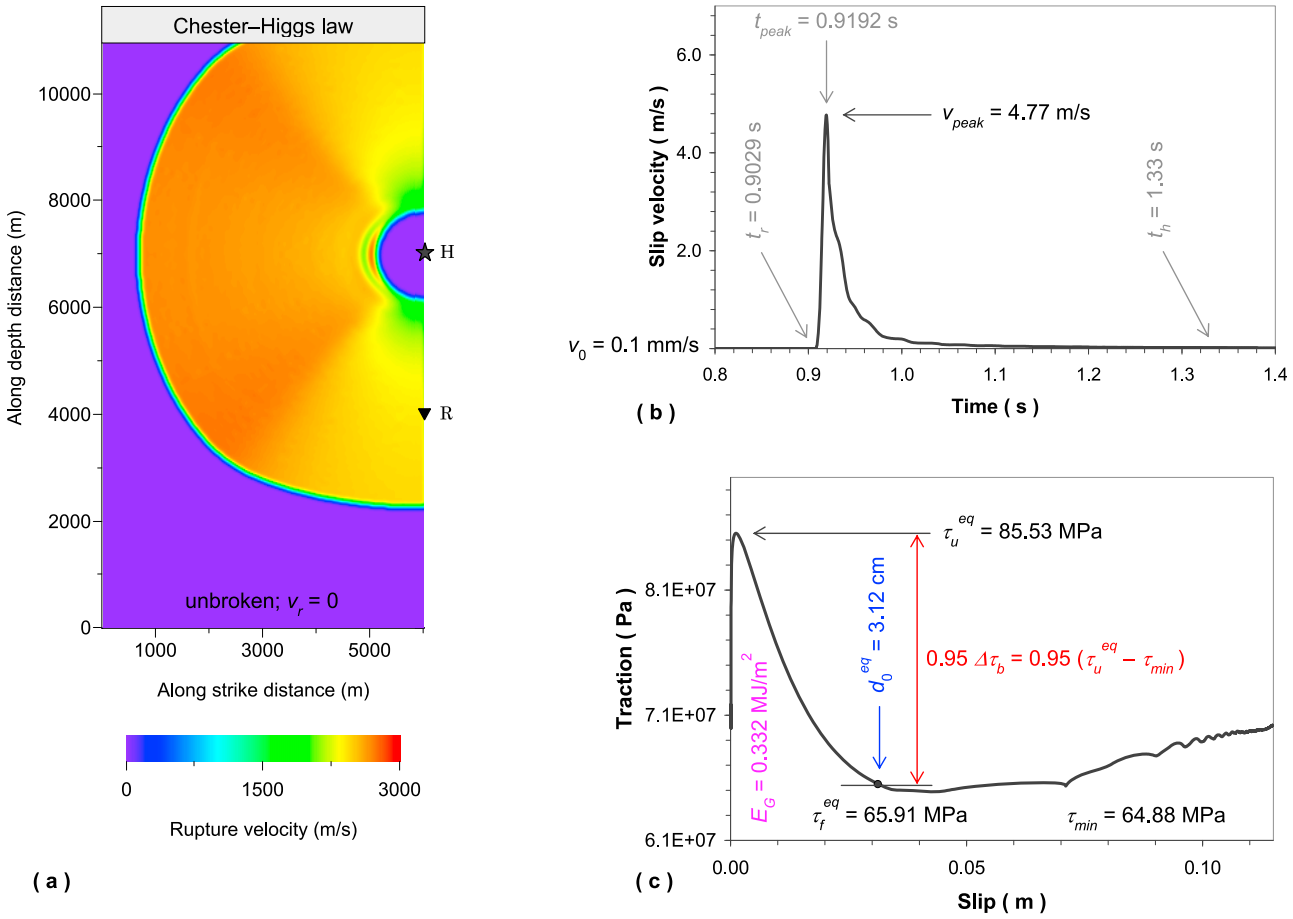

Figure 7. The same as in Figure 5, but now for a model predicting the healing of slip (i.e., a pulse-like rupture). The adopted governing model is a Ruina-Dieterich law with an additional explicit dependence on the temperature [see *Bizzarri*, 2011b, equation (48)].

exactly what we did in the case of the crack-like rupture; see section 6.2; from equation (6) we have: $t_R = 3.42 \times 10^{-2}$ s, which corresponds to an effective pulse duration of 4.70×10^{-2} s (i.e., $\sim t_{pulse}/9$). The result is plotted as thin red curve in Figure 8a. We note that both these two choices verify the condition $t_R > 2\, t_S$ so that the analytical expression of the MY SVF as in equation (1) is the correct one.

7.3. Representation Through the B Function

[47] From Figure 7c we have the estimate of the levels of stress, fracture energy density and slip-weakening distance for the spontaneous model, as well that of the breakdown stress drop ($\Delta\tau_b = \tau_u^{eq} - \tau_{\min}$ =20.65 MPa; see Figure 7c). Additionally, also v_0 is known (see Figure 7b). From equation (21) we obtain: $k = 1.86 \times 10^8$ Pa/m, which is lower than the upper bound of $\Delta\tau_b/d_0$ in equation (18) (note that this is simply because $u_{tot} > d_0$; see Figure 7c). On the other hand, the parameter m can be retrieved from equation (22), by putting $l = v_S\, t_{pulse}$, as discussed in section 4; since t_{pulse} = 0.4271 s we have: $m = 3.84 \times 10^6$ Kg/m^2. Remembering that $T = 2\pi\sqrt{m/k}$, we finally obtain: T = 0.902 s. With this choice, however, we would obtain a too long pulse; by keeping T = 0.08 s (which is the smallest period guaranteeing that the conditions in equation (17) are satisfied for the given parameters and for the above-mentioned value of k) we obtain the result is reported in blue in Figure 8a; note that we apply a time shift, in order to have at $t = t_r$ = 0.9029 s the first value of $v^{(B)}$ exceeding v_l = 0.1 m/s (which formally defines the rupture time in the spontaneous model [see also *Bizzarri and Belardinelli*, 2008, and references therein]).

7.4. Discussion

[48] The most apparent result emerging from Figure 8a is that both the MY and B the functions (thick red and blue curves, respectively) differ from the spontaneous dynamic solution (black curve); in particular, both of them underpredict v_{peak} We can see that the MY SVF predicts a too slow deceleration phase with respect to the 3-D solution. We also mention that with the MY function it is possible to better reproduce v_{peak}, as described in section 7.2, but in this case the pulse will result significantly shorter than the solution from the 3-D model; from the thin red line in Figure 6a we have that the deceleration phase is now too rapid compared to the spontaneous solution and only the sharp peak of the spontaneous solution is fitted by the analytical solution.

[49] In spite of the above-mentioned discrepancies, all the SVF are able to exactly capture the final slip in this fault receiver, as it is visible from the inset of Figure 8a. This is not surprising in the case of MY (where u_{tot} is in fact an input

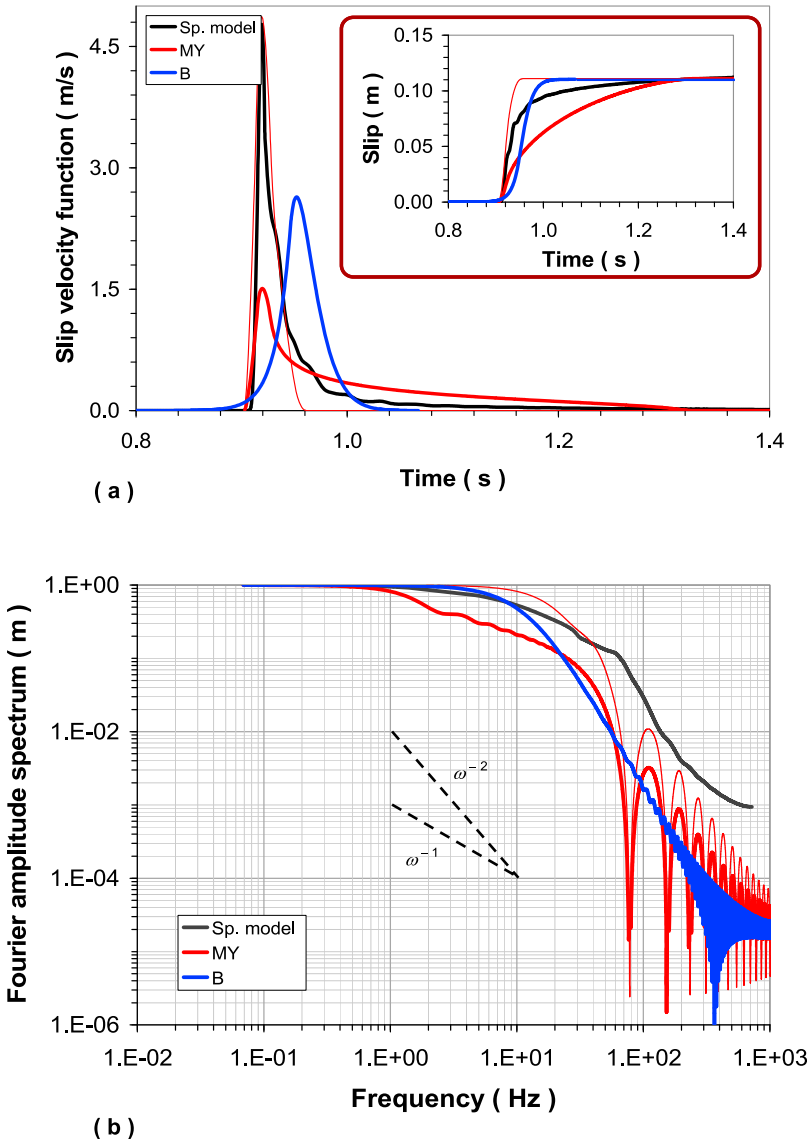

Figure 8. (a) Comparison between the fault slip velocity in the receiver R for the spontaneous pulse-like model of Figure 7 against the MY and the B SVF. (b) Comparison between the resulting Fourier amplitude spectra. The thin curve is an alternative parameterization of the MY, which preserve the peak slip velocity, but not the pulse duration (see section 7.2 for details).

parameter), but it is a nontrivial result for the B SVF, for which the total slip cannot be explicitly controlled a priori.

[50] Moreover, we can clearly see that the most gentle acceleration phase is predicted by the B function, where the increasing part of the slip rate history is not so sharp as in the other cases. Indeed, we recall that the B function is a solution pertaining to a 1-D spring-slider analog dashpot model, in which the system is loaded only by the external load of tectonic origin (expressed as $k\, v_0\, t$). On the contrary, in a 3-D fault model the considered node is also subject to the so-called restoring forces, which physically represent the dynamic load due to the redistribution of stress caused by the neighboring points that are already slipping. This load is known to have relevant effects in the dynamics of the system, as discussed in *Bizzarri and Belardinelli* [2008]. As a net result, during the dynamic motion the B function neglects, by definition, the contribution of such an additional load and this can explain the more slow acceleration and the lower peak in v.

[51] From the FAS of these time histories (Figure 8b) we can see that at low frequencies (i.e., below 10 Hz) the FAS $v^{(B)}$ approximates very well the FAS $v^{(\text{sp. model})}$. We remark here that in the case of crack-like function we did not observe such a good agreement, in terms of frequency content, with none of the considered SVF (see Figure 6b). Another interesting outcome of our results is that above 20 Hz the B function has a reduced high frequency content with respect to the MY SVF, as already found (see Figures 3 and 4b). For frequencies greater than 30 Hz the spectra roughly behave as ω^{-2}, in agreement with previous findings. Remarkably, the fall off at high frequencies of the SVF agrees quite well with the spontaneous model. Moreover, an interesting feature of all the spectra is a flattening in the final

portion of it, at frequencies greater than 400 Hz. However, we remark that his portion of the spectra is very far from the resolution of the recorder signals of real earthquakes and also above the resolution of the model achieved with the present computation capabilities.

8. Application to a Heterogeneous Earthquake Event

[52] The homogeneous models presented in sections 6 and 7 have to be regarded as idealizations of the true behavior of a crustal earthquake. Indeed, we know that complex geometries (such as bending and branching), fault segmentation and rheological heterogeneities can play a central role in the origin of the slip complexity on the fault surface and in the high frequencies content of the recorded seismograms [see also *Madariaga*, 1983]. The heterogeneities of the fault properties are responsible of possible multiple slipping as well as of very complex patterns of slip (and slip velocity) distribution, which will definitively affect the spectral properties of the time histories.

[53] In this section we consider a heterogeneous model where a linear slip-weakening friction law [*Bizzarri*, 2011b, equation (25)] is assumed to govern the fault. The initial shear stress is not uniform, as in previous cases (see sections 6.1 and 7.1), but it is characterized by a magnitude which decays as k^{-1} at high spatial wave numbers k [see *Bizzarri and Spudich*, 2008, Figure 11a]. Namely, its spatial spectral density follows *Bizzarri* [2010b, equation (21)].

[54] To perform the comparison between the numerical solution and the predictions from the analytical SVF we select three fault receivers, where the rupture speed is lower than the S wave speed. Then we determine the parameters of the SVF exactly as described in the previous section 7 and summarized in Table 3. There is no reason to overemphasize that the procedure described in Table 3 is sufficiently general to be applied in many different receivers and configurations.

[55] The results of our comparison are reported in Figure 9, where the black lines still refer to the spontaneous modeling, the red lines refer to the MY and the gray lines refer to the PR function. In a heterogeneous configuration it is possible to have multiple slipping episodes (clearly denoted by the multiple peaks of fault slip velocity in Figures 9b and 9c), which correspond to further stress releases. With a single analytical function is impossible to fit all these details (as well as their high frequency content), and therefore we decided to focus on the first peak of v, which formally represents the primary rupture front defining the rupture onset in a given fault receiver. We can see that there is a serious mismatch in the frequency domain between the analytical functions and the numerical solutions. This is rather obvious, due to the analytical nature of the SVF. Nevertheless we can see that the MY is able to fit the peak in v, in terms of amplitude and duration. This is not obvious, since the MY — we recall it again — formally pertain to a pulse-like solution. Another interesting conclusion emerging from this analysis is that, in general, the MY performs better than the PR, especially when v_{peak} is high (see Figure 9a). We cannot exclude that an ad hoc tuning of the parameter $\Delta\tau_b$ will better fit to numerical solution, but it would be a completely arbitrary choice; we use exactly the value of the breakdown stress drop inferred from the spontaneous model. At the same time, the decelerating phase of the rupture (i.e., the decreasing part of the first peak of v) is reproduced only qualitatively by the SVF.

[56] Overall, we can therefore conclude that in the presence of the frictional heterogeneities we are unable to fit (at least with a single analytical function) all the details of a numerical solution pertaining to a spontaneous rupture, especially in the frequency domain. In general, we have seen that the MY SVF exhibits a better agreement with respect to the PR function, especially considering the amplitude of the peak slip velocity corresponding to the rupture front and the first part of its decrease.

9. Conclusions

[57] In this paper we have considered three different slip velocity functions (SVF), which describe the time evolution of the fault slip velocity; the first is the so-called modified Yoffe function (MY SVF; equation (1)), which comes from the singular crack solution from *Broberg* [1978, 1999] and *Freund* [1979], the second (PR SVF; equation (12)) derives from the solution of *Palmer and Rice* [1973] for a non-spontaneous crack obeying a position-weakening constitutive model and the third is the solution (B SVF; equation (15)) for a 1-D spring-slider model subject to a linear slip-weakening friction law. All of them are based upon theoretical arguments, described in detail in previous sections 2 to 4, and they do not are merely analytical equations used in kinematic modeling of faults. It is important to state an important restriction in these formulations; they are appropriate to describe subshear ruptures, but they cannot tell anything about the supershear regime.

[58] As summarized in Table 1, the above-mentioned SVF depend on some parameters. The MY is characterized only by the duration of the pulse, the acceleration time and the total cumulative slip. The PR and the B SVF depend on quantities more strictly related to the energetics of the rupture; the fracture energy density, the breakdown stress drop or the rupture speed, as well as one the physical properties of the medium where the fault is embedded (see Table 1). Indeed, the adoption of a SVF described by few free parameters makes the inversion of strong motion data more stable as compared to the multiple time window technique that is frequently used [e.g., *Hartzell and Heaton*, 1983; *Wald and Heaton*, 1994; *Sekiguchi et al.*, 1996]. On the other hand the explicit control in the SVF of the most relevant parameters which characterize a dynamic rupture make more physically robust the comparison with a solution arisen from spontaneous dynamic models.

[59] In this paper we have first scrutinized the properties of all the three SVF; first of all we have discussed their most important features and their shortcomings, basically focusing on the prediction of the peak slip velocity (v_{peak}) and the pulse duration. A synoptic review is also summarized in Table 1. Then, by considering the same parameters, we have quantitatively compared the various SVF (section 5). An important outcome emerging from this analysis is that the time evolutions of the slip and slip velocity predicted by the MY and B functions are very similar, while the PR predicts a very sharp peak (which corresponds to a smaller cumulative slip; see Figure 1). Correspondingly, the PR SVF is richer in high frequency and the fall off of its spectrum at high

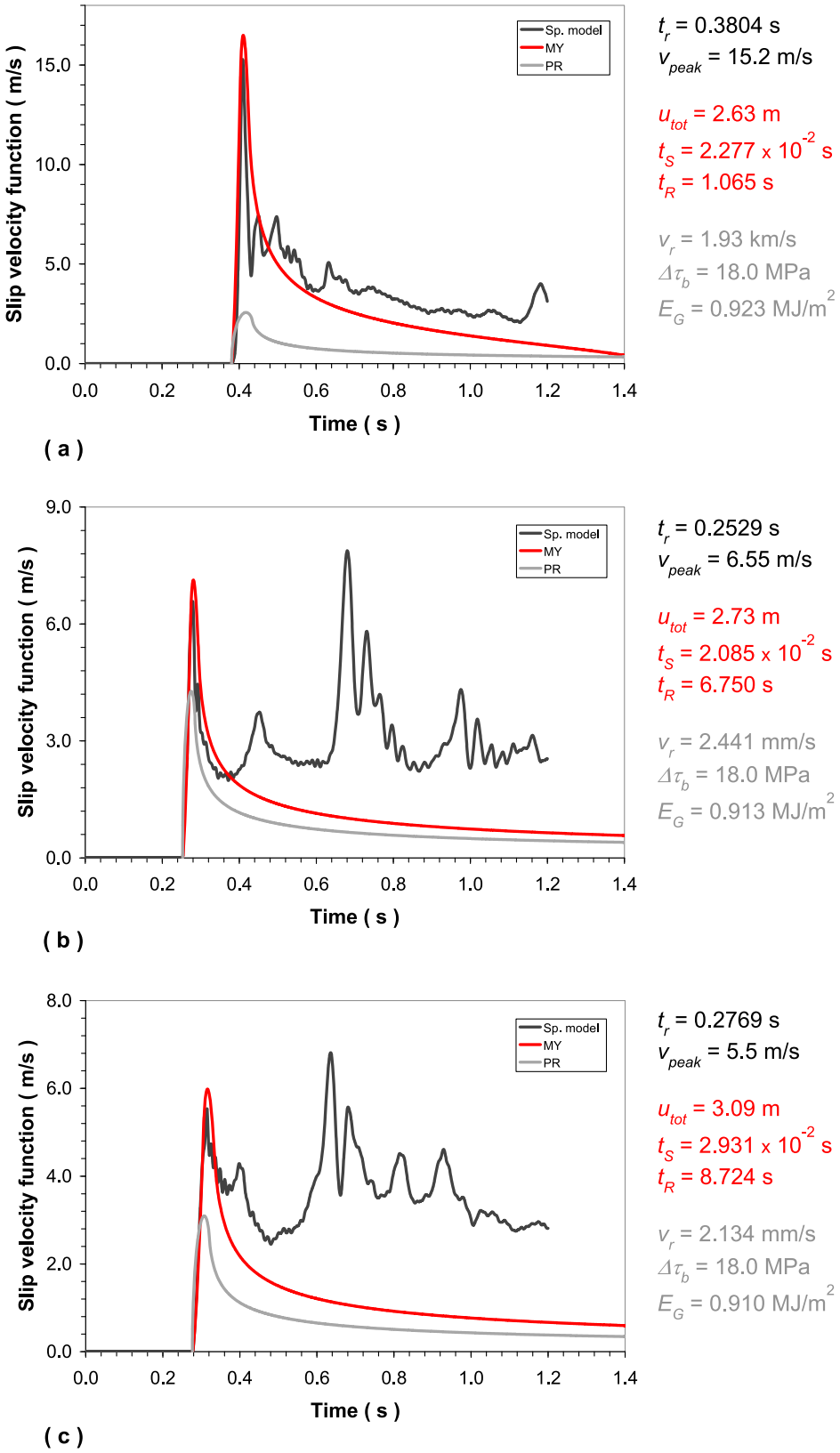

Figure 9. Results pertaining to a heterogeneous earthquake model (described in detail in section 8). Black curves refer to the spontaneous model, red curves to the MY SVF and the gray curves to the PR SVF. The absolute coordinates of the receivers (reader can refer to *Bizzarri and Spudich* [2008, Figure 11a] for the representation of the fault plane) are (a) (3.2,2.4) km, (b) (2.4,3.2) km and (c) (4.8,4.0) km. All the parameters of the different SVF are reported for each panel.

frequencies goes roughly as $\omega^{-1.5}$, while those of MY and B more closely follows ω^{-2} (see Figure 3). This mismatch is not surprising, in that PR function describes a crack-like rupture, while the other two SVF are appropriate to describe a pulse-like rupture, where the slip heals after some time. A better agreement with the three SVF can be obtained by choosing ad hoc values of some parameters of the PR function (see Figure 4a), which guarantees a more similar time evolution of both u and v and a less different FAS (Figure 4b).

[60] We have then tried to reproduce a given slip velocity time history, as resulting from a spontaneous modeling of a 3-D fault obeying different friction laws, either rate- and state-dependent or linear slip-weakening, by using the three SVF. We have considered rather different models, two subshear ruptures which homogeneous rheological properties (one representing a crack-like and the other one representing a pulse-like rupture; sections 6 and 7, respectively) and a highly heterogeneous rupture (section 8). In all cases we have described in detail how it is possible to retrieve the input parameters of the different SVF from the given time evolution of v; see sections 6.2, 6.3, 7.2, 7.3. In Table 3 we have reported a compendious summary describing this procedure, which is sufficiently general to be applied to an arbitrary, single instance rupture event. With this kind of comparison we aimed to explore if, for prescribed dynamic parameters which characterize a spontaneous earthquake model, the various SVF considered are able to reproduce the behavior of v as resulting from the forward, spontaneous modeling.

[61] In the case of a crack-like rupture (section 6) it emerges that the PR function fits very well the occurrence of v_{peak} and it reproduces well the final, asymptotic value of v (see Figure 6a). Surprisingly, also the MY is able to describe the behavior of v, if we restrict our analysis to the time window in which $v^{(MY)}$ is nonzero. Moreover, the peak of v predicted by the BY SVF (which also fits the time of its occurrence, by construction) is in a good agreement with that obtained from the spontaneous model. For frequencies below 30 Hz the spectra of these two SVF are poorer in frequency content with respect to that of the spontaneous solution (see Figure 6b). At higher frequencies the fall offs of the spectra exhibit some differences; both the 3-D model and the MY roughly decay as ω^{-2}, while the FAS of PR function goes like $\omega^{-1.5}$. These behavior are in agreement with previous findings (see Figures 3 and 4b).

[62] In the case of pulse-like rupture (section 7) both the MY and the B functions are able to reproduce the final slip (see the inset plot in Figure 8a); this is not surprising in the case of the MY (in which u_{tot} is an input parameter), but is interesting in the case of the B function, where u_{tot} is not prescribed a priori, but it results as a part of the solution. Nevertheless, both these two SVF underpredict v_{peak} (see Figure 8a). The agreement would be better if we require the MY to reproduce v_{peak}, by exploiting equation (6); in this case, however, the resulting risetime (i.e., the duration of the slip velocity pulse) is shorter compared to the spontaneous solution (thin red line in Figure 8a). We also mention that the MY better agrees with the rapid accelerating phase predicted by the 3-D model. On the contrary, the B function predicts a gentle slip acceleration and this is mainly due to the fact that this SVF comes from a 1-D spring-slider dashpot model, which by definition neglects the dynamic load due to the other slipping points of the fault, thus reducing the total load acting on the target point [see also *Bizzarri and Belardinelli*, 2008]. Remarkably, for frequencies lower than 10 Hz the spectrum of B function is practically indistinguishable from that of the spontaneous model (see Figure 8b). For $\omega > 20$ Hz, we have that FAS $v^{(B)}$ < FAS $v^{(MY)}$, as in previous Figures 3 and 4b. For $\omega > 30$ Hz all the spectra roughly go as ω^{-2}.

[63] To summarize, we have seen that none of the considered SVF is able to reproduce exactly each single details of the slip velocity time histories obtained from a dynamic spontaneous model. This is particularly true in the case of heterogeneous configurations, where it is impossible to fit, with a single analytical function, all the details of the spontaneous solution, which is characterized by multiple peaks accounting for multiple stress drops (see Figure 9). Nevertheless, we have shown that: *i*) The MY and the PR SVF can reproduce adequately well the main features of a dynamic solution in the case of a crack-like rupture (Figure 6a). *ii*) In the case of a pulse-like rupture both the MY and the B SVF tend to underestimate v_{peak}, but all of them capture very well the final cumulated fault slip. Due to its 1-D nature the B function predicts a too gentle acceleration phase, but it fits well the decelerating phase of the pulse (Figure 8a). However, the B function fits better that the MY the overall behavior of the fault slip (inset in Figure 8a). *iii*) The considered SVF are able to reproduce the spectral fall off of a 3-D solution at intermediate frequencies (namely $\omega < 20$ Hz), the MY and the PR for a crack-like rupture, the MY and the B SVF for a pulse-like rupture (see Figures 6b and 8b, respectively). In particular, for $\omega < 10$ Hz the spectral content of the B function is practically indistinguishable from that of the spontaneous solution. *iv*) At high frequencies the spectra decays roughly as ω^{-2}, with the exception of the PR function, which goes like $\omega^{-1.5}$ (see Figures 6b and 8b). *iv*) In the case of heterogeneous ruptures the MY is able to capture the main behavior of the first peak in v, pertaining to the rupture tip, and the first part of its decrease. Although there is an obvious mismatch in the frequency domain, the MY is able to reproduce the amplitude and the duration of the numerical solutions. On the contrary, for the dynamic parameter characterizing the spontaneous model, the PR SVF tend to underpredict v_{peak}, as well as the decelerating phase of the first peak.

[64] The choice of a source time function to be used in the kinematic description of faults is arbitrary, but at the same time it is of pivotal importance in the contest of hazard assessment and ground motions generation [e.g., *Hisada*, 2000, 2001; *Guatteri et al.*, 2003; *Page et al.*, 2005]. The thorough analysis of the three theoretically-based SVF performed in this paper is inserted in this framework. We emphasize the band-limited inversions rely on low frequency ranges (roughly up to 1 Hz). In that range the details of the shape of the SVF can be less influents than in the high frequency ranges (typical of strong motion generation). However, we found that for a crack-like rupture the FAS of the MY and of the PR functions are different also at low frequencies (see Figure 6b). Moreover, we are not aware that possible geometrical irregularities, stress heterogeneities, free surface effects and attenuation can definitively smear the details of the analytical functions.

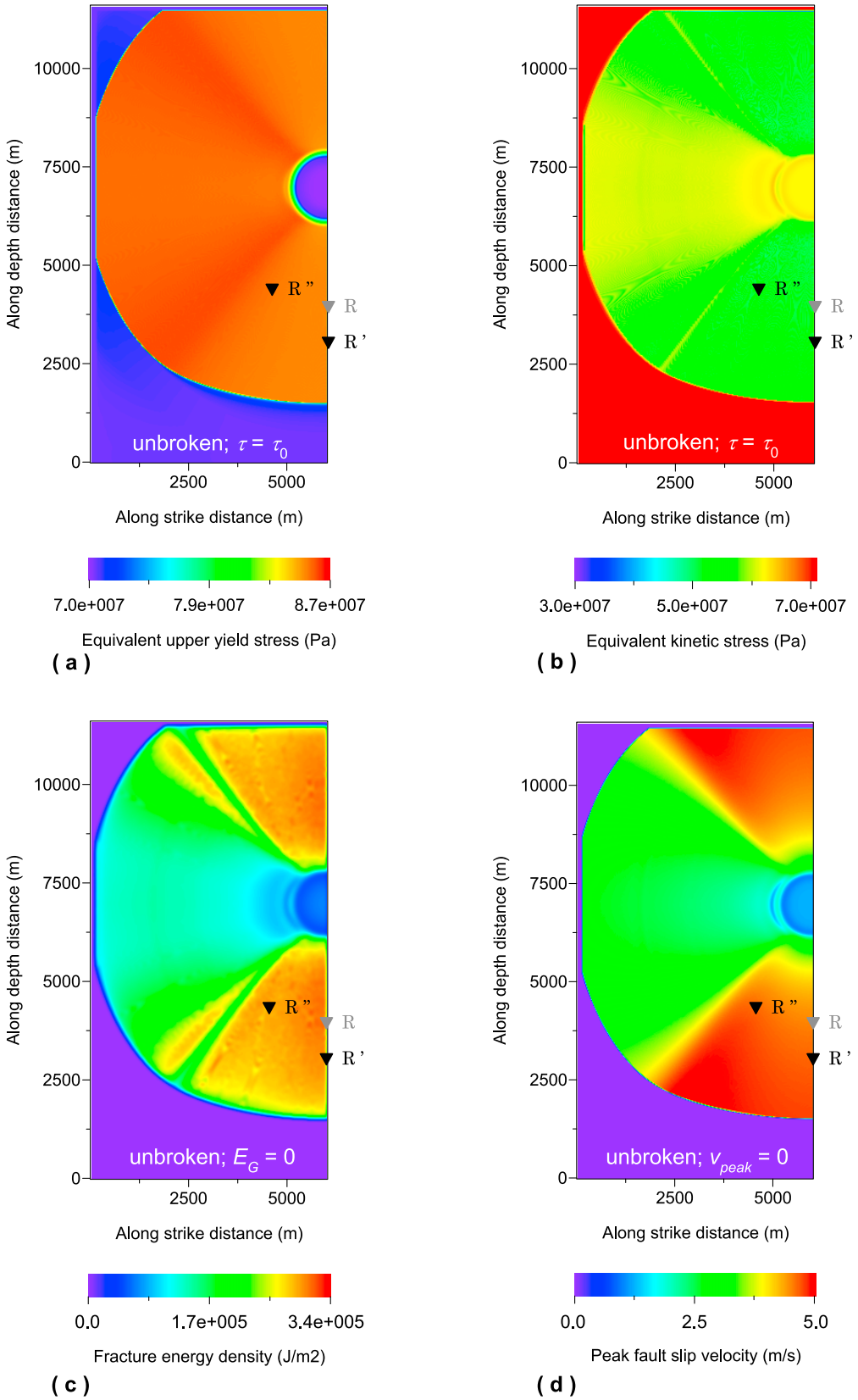

Figure A1. Spatial distribution on the fault plane of the relevant physical observables pertaining to the model of Figures 7 and 8. (a) Equivalent upper yield stress (τ_u^{eq}). (b) Equivalent kinetic friction level (τ_f^{eq}). (c) Fracture energy density (E_G). (d) Peak fault slip velocity (v_{peak}). The locations of R′ (used in Figure A2) and R (used in Figure A3) are marked in all panels. For completeness we also report (in gray) the location of the receiver R used in Figures 5–8.

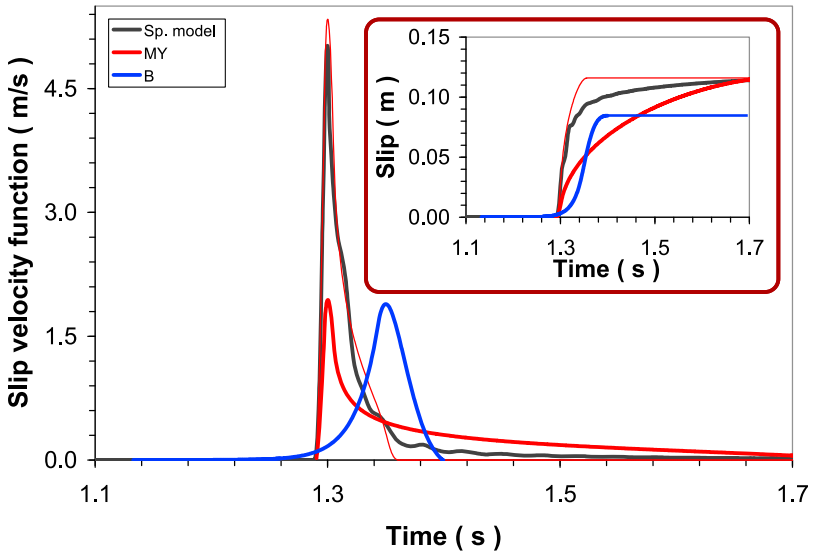

Figure A2. The same as Figure 8a, but now for a receiver R located at a distance of 4 km from H.

[65] The next step of this research, which will be the matter of a separate study, is to perform kinematic models by adopting these SVF and see how the resulting traction evolution differs from that used to constrain their input parameters.

Appendix A: Results Pertaining to Different Receivers on the Fault

[66] In sections 6 and 7 we have compared the result pertaining to a dynamic spontaneous model with the various SVF considered in this paper by focusing, for each single rupture model, either crack-like or pulse-like, on a fault receiver having the same strike coordinate of the hypocenter.

[67] In the framework of the slip-weakening model the levels of stresses are prescribed, as well as the characteristic slip distance and therefore both $\Delta\tau_b$ and E_G are constant over the whole fault. In the case of rate- and state-dependent rheology, we cannot exclude a priori some fluctuations in the above-mentioned quantities from point to point, in that the levels of stresses are not imposed as input parameters [e.g., *Bizzarri and Cocco*, 2003].

[68] In order to explore the level of variability in the case of a homogeneous rupture we plot in Figure A1 the spatial distributions of the equivalent upper yield stress (τ_u^{eq}), the equivalent kinetic friction level (τ_f^{eq}), the resulting fracture energy density (E_G) and the peak fault slip velocity (v_{peak}) in the case of the model presented in section 7. The results are qualitatively unchanged also in the case of the model presented in section 6.

[69] By looking at Figure A1 we can see that the variations of the physical observables occurs if we compare receivers aligned along the strike direction (where the propagation is basically mode II) with receivers aligned along the depth (where the propagation is basically mode III). This is particularly true if we consider τ_f^{eq} (Figure A1b), E_G (Figure A1c) and v_{peak} (Figure A1d), as τ_u^{eq} (Figure A1a) exhibits even smaller variations from point to point. The increase of v_{peak} for increasing distances from the hypocenter along the strike direction is intimately related to the so-called shrinking of the cohesive zone [*Andrews*, 1976; *Bizzarri et al.*, 2001]. More importantly, if we look at receivers located at the strike coordinate of the hypocenter and aligned along the depth, we can observe that all the observables have roughly the same values. We recall here that this is the appropriate profile where the all the three different analytical SVF have to be compared against the numerical solution from a spontaneous rupture model (the B function comes from an equation of motion which is appropriate for mode III propagation; see details in *Bizzarri* [2012b]).

[70] In Figure A2 we select a fault receiver located at a distance of 4 km from the hypocenter along the depth. The location of this new fault receiver R is reported in Figure A1. In this case v_{peak} = 5.02 m/s (instead of 4.77 m/s, as in Figure 7b), ad t_{pulse} = 0.46 s. We proceed exactly as done in section 7, by following the scheme of Table 3; for the MY SVF we have the following parameters u_{tot} = 0.116 m, $t_S = 7.69 \times 10^{-3}$ s and t_R = 0.4446 s (thick red curve in Figure A2). As for the receiver of Figures 7 and 8 we can clearly see that these parameters predict and underestimate of v_{peak} arising from the spontaneous model. If we constrain v_{peak} instead of the pulse duration, then we obtain $t_R = 5.62 \times 10^{-2}$ s, which gives a better fit of the time history of v given by the dynamic model (see thin red curve in Figure A2). Concerning the B function the conclusions are exactly the same as in section 7; if we set $k = 2.18 \times 10^6$ Pa/m (from equation (21)) and $m = 3.84 \times 10^6$ Kg/m^2 (from equation (22)) we would obtain a too long pulse. On the contrary, if we set T = 0.09 s (which is the smallest value which guarantees that the conditions in equation (17) are satisfied for the given dynamic parameters and for the above-mentioned value of k) we obtain the blue curve reported in Figure A2. As for the receiver shown in Figure 8a, also in this case the B SVF gives a underestimate of v_{peak} and again the pulse duration is larger than that emerging from the spontaneous solution.

[71] We have also considered an additional receiver R (also reported in Figure A1), which is at a distance of 3 km from the hypocenter, but is now aligned in the direction of the mixed-mode 45° profile. We proceed exactly as in the previous example and the results are reported in Figure A3.

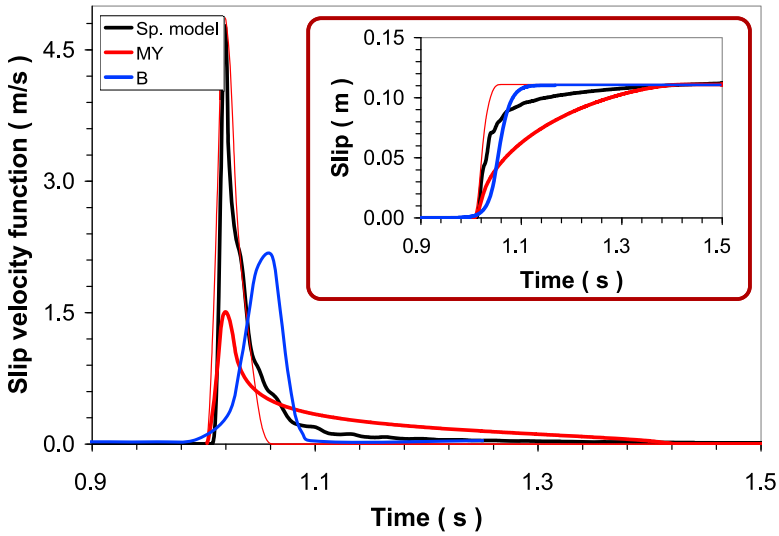

Figure A3. The same as Figure 8a, but now for a receiver R′ still located at a distance of 4 km from H, but along the mixed-mode 45° direction.

We can clearly see that the conclusions are the same as in the previous case.

[72] In conclusion, we have seen that this exercise confirms the two main conclusions discussed in section 7; the best estimate of the shape of the spontaneous solution is given by the MY SVF, by constraining u_{tot} and v_{peak} instead of u_{tot} and t_{pulse}. Moreover, the B function, even with the ad hoc calibration of the parameter T — or analogously of the parameter m — gives a underestimate of v_{peak} and a larger slip duration (and correspondingly a smaller value of the total cumulative slip; see inset in Figure A2).

[73] **Acknowledgments.** I thank the Editor, R. Nowack, an anonymous Associate Editor and two anonymous reviewers for their stimulating comments.

References

Andrews, D. J. (1976), Rupture velocity of plane strain shear cracks, *J. Geophys. Res.*, *81*(32), 5679–5687, doi:10.1029/JB081i032p05679.

Andrews, D. J. (1994), Dynamic growth of mixed–mode shear cracks, *Bull. Seismol. Soc. Am.*, *84*(4), 1184–1198.

Bizzarri, A. (2009a), Can flash heating of asperity contacts prevent melting?, *Geophys. Res. Lett.*, *36*, L11304, doi:10.1029/2009GL037335.

Bizzarri, A. (2009b), What does control earthquake ruptures and dynamic faulting? A review of different competing mechanisms, *Pure Appl. Geophys.*, *166*, 741–776, doi:10.1007/s00024-009-0494-1.

Bizzarri, A. (2010a), Pulse-like dynamic earthquake rupture propagation under rate-, state- and temperature-dependent friction, *Geophys. Res. Lett.*, *37*, L18307, doi:10.1029/2010GL044541.

Bizzarri, A. (2010b), On the relations between fracture energy and physical observables in dynamic earthquake models, *J. Geophys. Res.*, *115*, B10307, doi:10.1029/2009JB007027.

Bizzarri, A. (2011a), Dynamic seismic ruptures on melting fault zones, *J. Geophys. Res.*, *116*, B02310, doi:10.1029/2010JB007724.

Bizzarri, A. (2011b), On the deterministic description of earthquakes, *Rev. Geophys.*, *49*, RG3002, doi:10.1029/2011RG000356.

Bizzarri, A. (2012a), Rupture speed and slip velocity: What can we learn from simulated earthquakes?, *Earth Planet. Sci. Lett.*, *317–318*, 196–203, doi:10.1016/j.epsl.2011.11.023.

Bizzarri, A. (2012b), Modeling repeated slip failures on faults governed by slip-weakening friction, *Bull. Seismol. Soc. Am.*, *102*(2), 812–821, doi:10.1785/0120110141.

Bizzarri, A. (2012c), The mechanics of lubricated faults: Insights from 3-D numerical models, *J. Geophys. Res.*, *117*, B05304, doi:10.1029/2011JB008929.

Bizzarri, A., and M. E. Belardinelli (2008), Modelling instantaneous dynamic triggering in a 3–D fault system: Application to the 2000 June South Iceland seismic sequence, *Geophys. J. Int.*, *173*, 906–921, doi:10.1111/j.1365-246X.2008.03765.x.

Bizzarri, A., and M. Cocco (2003), Slip-weakening behavior during the propagation of dynamic ruptures obeying rate- and state-dependent friction laws, *J. Geophys. Res.*, *108*(B8), 2373, doi:10.1029/2002JB002198.

Bizzarri, A., and M. Cocco (2005), 3D dynamic simulations of spontaneous rupture propagation governed by different constitutive laws with rake rotation allowed, *Ann. Geophys.*, *48*(2), 279–299.

Bizzarri, A., and P. Spudich (2008), Effects of supershear rupture speed on the high-frequency content of *S* waves investigated using spontaneous dynamic rupture models and isochrone theory, *J. Geophys. Res.*, *113*, B05304, doi:10.1029/2007JB005146.

Bizzarri, A., M. Cocco, D. J. Andrews, and E. Boschi (2001), Solving the dynamic rupture problem with different numerical approaches and constitutive laws, *Geophys. J. Int.*, *144*, 656–678, doi:10.1046/j.1365-246x.2001.01363.x.

Bouchon, M. (1981), A simple method to calculate Green's function for layered media, *Bull. Seismol. Soc. Am.*, *71*, 959–971.

Broberg, K. (1978), On transient sliding motion, *Geophys. J. R. Astron. Soc.*, *52*, 397–432, doi:10.1111/j.1365-246X.1978.tb04240.x.

Broberg, K. (1999), *Cracks and Fracture*, 752 pp., Academic, San Diego, Calif.

Burridge, R. (1973), Admissible speeds for plane-strain self-similar shear cracks with friction but lacking cohesion, *Geophys. J. R. Astron. Soc.*, *35*, 439–455, doi:10.1111/j.1365-246X.1973.tb00608.x.

Cao, T., and K. Aki (1986), Seismicity simulation with a rate- and state-dependent friction, *Pure Appl. Geophys.*, *124*(3), 487–513, doi:10.1007/BF00877213.

Cotton, F., and M. Campillo (1994), Application of seismogram synthesis to the study of earthquake source from strong motion records, *Ann. Geophys.*, *37*(6), 1539–1564.

Freund, L. B. (1979), The mechanics of dynamic shear crack propagation, *J. Geophys. Res.*, *84*, 2199–2209, doi:10.1029/JB084iB05p02199.

Fukuyama, E., T. Mikumo, and K. B. Olsen (2003), Estimation of the critical slip-weakening distance: Theoretical background, *Bull. Seismol. Soc. Am.*, *93*, 1835–1840, doi:10.1785/0120020184.

Guatteri, M., P. M. Mai, G. C. Beroza, and J. Boatwright (2003), Strong ground-motion prediction from stochastic-dynamic source models, *Bull. Seismol. Soc. Am.*, *93*(1), 301–313, doi:10.1785/0120020006.

Hartzell, S. H., and T. H. Heaton (1983), Inversion of strong ground motion and teleseismic waveform data for the fault rupture history of the 1979 Imperial Valley, California, earthquake, *Bull. Seismol. Soc. Am.*, *73*, 1553–1583.

Hisada, Y. (2000), A theoretical omega-square model considering the spatial variation on slip and rupture velocity, *Bull. Seismol. Soc. Am.*, *90*, 387–400, doi:10.1785/0119990083.

Hisada, Y. (2001), A theoretical omega-square model considering the spatial variation on slip and rupture velocity. II. Case for a two dimensional

source model, *Bull. Seismol. Soc. Am.*, *91*, 651–666, doi:10.1785/0120000097.

Kostrov, B. V. (1964), Self-similar problems of propagation of shear cracks, *J. Appl. Math. Mech.*, *28*, 1077–1087, doi:10.1016/0021-8928(64)90010-3.

Kostrov, B. V. (1974), Crack propagation at variable velocity, *J. Appl. Math. Mech.*, *38*(3), 551–560.

Liu, P., and R. J. Archuleta (2004), A new nonlinear finite fault inversion with three-dimensional Green's functions: Application to the 1989 Loma Prieta, California, earthquake, *J. Geophys. Res.*, *109*, B02318, doi:10.1029/2003JB002625.

Madariaga, R. (1983), High frequency radiation from dynamic earthquake fault models, *Ann. Geophys.*, *1*, 17–23.

Mikumo, T., K. B. Olsen, E. Fukuyama, and Y. Yagi (2003), Stress-breakdown time and slip-weakening distance inferred from slip-velocity functions on earthquake faults, *Bull. Seismol. Soc. Am.*, *93*, 264–282, doi:10.1785/0120020082.

Nakamura, H., and T. Miyatake (2000), An approximate expression of slip velocity time functions for simulation of near–field strong ground motion (in Japanese with English abstract), *J. Seismol. Soc. Jpn.*, *53*, 1–9.

Nielsen, S., and R. Madariaga (2003), On the self–healing fracture mode, *Bull. Seismol. Soc. Am.*, *93*, 2375–2388, doi:10.1785/0120020090.

Ohnaka, M., and L. Shen (1999), Scaling of the shear rupture process from nucleation to dynamic propagation: Implications of geometric irregularity of the rupturing surfaces, *J. Geophys. Res.*, *104*(B1), 817–844, doi:10.1029/1998JB900007.

Ohnaka, M., and T. Yamashita (1989), A cohesive zone model for dynamic shear faulting based on experimentally inferred constitutive relation and strong motion source parameters, *J. Geophys. Res.*, *94*, 4089–4104, doi:10.1029/JB094iB04p04089.

Ohnaka, M., Y. Kuwahara, and K. Yamamoto (1987), Constitutive relations between dynamic physical parameters near a tip of the propagating slip zone during stick–slip shear failure, *Tectonophysics*, *144*, 109–125, doi:10.1016/0040-1951(87)90011-4.

Page, M. T., E. M. Dunham, and J. M. Carlson (2005), Distinguishing barriers and asperities in near–source ground motion, *J. Geophys. Res.*, *110*, B11302, doi:10.1029/2005JB003736.

Palmer, A. C., and J. R. Rice (1973), The growth of slip surfaces in the progressive failure of over-consolidated clay, *Proc. R. Soc. London, A*, *332*, 527–548, doi:10.1098/rspa.1973.0040.

Piatanesi, A., E. Tinti, M. Cocco, and E. Fukuyama (2004), The dependence of traction evolution on the earthquake source time function adopted in kinematic rupture models, *Geophys. Res. Lett.*, *31*, L04609, doi:10.1029/2003GL019225.

Poliakov, A. N. B., R. Dmowska, and J. R. Rice (2002), Dynamic shear rupture interactions with fault bends and off–axis secondary faulting, *J. Geophys. Res.*, *107*(B11), 2295, doi:10.1029/2001JB000572.

Rice, J. R. (1980), The mechanics of earthquake rupture, in *Physics of the Earth's Interior*, *Proc. Intl. School of Physics "E. Fermi", Course 18, 1979*, edited by A. M. Dziewonski and E. Boschi, pp. 555–649, North Holland, New York.

Scholz, C. H. (1990), *The Mechanics of Earthquakes and Faulting*, 439 pp., Cambridge Univ. Press, New York.

Sekiguchi, H., K. Irikura, T. Iwata, Y. Kachi, and M. Hoshiba (1996), Minute locating of faulting beneath Kobe and waveform inversion of source process during the 1995 Hyogo–ken Nanbu, Japan, earthquake using strong motion records, *J. Phys. Earth*, *44*, 473–487, doi:10.4294/jpe1952.44.473.

Tinti, E., A. Bizzarri, A. Piatanesi, and M. Cocco (2004), Estimates of slip weakening distance for different dynamic rupture models, *Geophys. Res. Lett.*, *31*, L02611, doi:10.1029/2003GL018811.

Tinti, E., E. Fukuyama, A. Piatanesi, and M. Cocco (2005), A kinematic source time function compatible with earthquake dynamics, *Bull. Seismol. Soc. Am.*, *95*(4), 1211–1223, doi:10.1785/0120040177.

Wald, D. J., and T. H. Heaton (1994), Spatial and temporal distribution of slip for the 1992 Landers, California, earthquake, *Bull. Seismol. Soc. Am.*, *84*, 668–691.

Walsh, J. B. (1971), Stiffness in faulting and in friction experiments, *J. Geophys. Res.*, *76*(35), 8597–8598, doi:10.1029/JB076i035p08597.

Yamashita, T. (1976), On the dynamical process of fault motion in the presence of friction and inhomogeneous initial stress. I: Rupture propagation, *J. Phys. Earth*, *24*, 417–444, doi:10.4294/jpe1952.24.417.

Yoffe, E. (1951), The moving Griffith crack, *Philos. Mag.*, *42*, 739–750.